Decadal Prediction Centers Prepare for a Major Volcanic Eruption

Reinel Sospedra-Alfonso, William Merryfield, Matthew Toohey, Claudia Timmreck, Jean-Paul Vernier, Ingo Bethke, Yiguo Wang, Roberto Bilbao, Markus Donat, Pablo Ortega, et al.

▶ **To cite this version:**

Reinel Sospedra-Alfonso, William Merryfield, Matthew Toohey, Claudia Timmreck, Jean-Paul Vernier, et al.. Decadal Prediction Centers Prepare for a Major Volcanic Eruption. Bulletin of the American Meteorological Society, 2024, 105 (12), pp.E2496-E2524. 10.1175/bams-d-23-0111.1 . hal-04943788

HAL Id: hal-04943788
https://hal.science/hal-04943788v1

Submitted on 14 Feb 2025

HAL is a multi-disciplinary open access archive for the deposit and dissemination of scientific research documents, whether they are published or not. The documents may come from teaching and research institutions in France or abroad, or from public or private research centers.

L'archive ouverte pluridisciplinaire **HAL**, est destinée au dépôt et à la diffusion de documents scientifiques de niveau recherche, publiés ou non, émanant des établissements d'enseignement et de recherche français ou étrangers, des laboratoires publics ou privés.

Distributed under a Creative Commons Attribution 4.0 International License

BAMS Article

Decadal Prediction Centers Prepare for a Major Volcanic Eruption

Reinel Sospedra-Alfonso,[a] William J. Merryfield,[a] Matthew Toohey,[b] Claudia Timmreck,[c] Jean-Paul Vernier,[d,e] Ingo Bethke,[f] Yiguo Wang,[g] Roberto Bilbao,[h] Markus G. Donat,[h,i] Pablo Ortega,[h] Jason Cole,[a] Woo-Sung Lee,[a] Thomas L. Delworth,[j] David Paynter,[j] Fanrong Zeng,[j] Liping Zhang,[j,k] Myriam Khodri,[l] Juliette Mignot,[l] Didier Swingedouw,[m] Olivier Torres,[l] Shuai Hu,[n] Wenmin Man,[n] Meng Zuo,[o] Leon Hermanson,[p] Doug Smith,[p] Takahito Kataoka,[q] and Hiroaki Tatebe[q,r]

KEYWORDS: Climate prediction; Operational forecasting; Climate models; Climate variability; Decadal variability; Aerosol radiative effect

ABSTRACT: The World Meteorological Organization's Lead Centre for Annual-to-Decadal Climate Prediction issues operational forecasts annually as guidance for regional climate centers, climate outlook forums, and national meteorological and hydrological services. The occurrence of a large volcanic eruption such as that of Mount Pinatubo in 1991, however, would invalidate these forecasts and prompt producers to modify their predictions. To assist and prepare decadal prediction centers for this eventuality, the Volcanic Response activities under the World Climate Research Programme's Atmospheric Processes and Their Role in Climate (APARC) and the Decadal Climate Prediction Project (DCPP) organized a community exercise to respond to a hypothetical large eruption occurring in April 2022. As part of this exercise, the Easy Volcanic Aerosol forcing generator was used to provide stratospheric sulfate aerosol optical properties customized to the configurations of individual decadal prediction models. Participating centers then reran forecasts for 2022–26 from their original initialization dates and, in most cases, also from just before the eruption at the beginning of April 2022, according to two candidate response protocols. This article describes various aspects of this APARC/DCPP Volcanic Response Readiness Exercise (VolRes-RE), including the hypothesized volcanic event, the modified forecasts under the two protocols from the eight contributing centers, the lessons learned during the coordination and execution of this exercise, and the recommendations to the decadal prediction community for the response to an actual eruption.

DOI: 10.1175/BAMS-D-23-0111.1

Corresponding author: Reinel Sospedra-Alfonso, reinel.sospedra-alfonso@ec.gc.ca

Manuscript received 18 May 2023, in final form 8 July 2024, accepted 19 August 2024

© 2024 American Meteorological Society. This published article is licensed under the terms of the default AMS reuse license. For information regarding reuse of this content and general copyright information, consult the AMS Copyright Policy (www.ametsoc.org/PUBSReuseLicenses).

Unauthenticated | Downloaded 02/14/25 09:04 AM UTC

SIGNIFICANCE STATEMENT: Decadal climate predictions crucially fill a gap between seasonal forecasts, which typically cover the coming 6–12 months, and long-term climate projections that extend to 2100 and beyond. Multimodel decadal predictions issued annually by the World Meteorological Organization are generally skillful but could be invalidated if a large climate-altering volcanic eruption like that of Mount Pinatubo in 1991 were to occur. These predictions can in principle be modified by each contributing center to include estimates of stratospheric aerosol radiative influences stemming from the eruption. However, an effective and timely response requires planning and international coordination. This paper describes an effort to develop such a framework through a practical exercise under which decadal prediction centers respond to a hypothetical major eruption.

AFFILIATIONS: [a] Canadian Centre for Climate Modelling and Analysis, Environment and Climate Change Canada, Victoria, British Columbia, Canada; [b] Institute of Space and Atmospheric Studies, University of Saskatchewan, Saskatoon, Saskatchewan, Canada; [c] Max-Planck-Institut für Meteorologie, Hamburg, Germany; [d] National Institute of Aerospace, Hampton, Virginia; [e] NASA Langley Research Center, Hampton, Virginia; [f] Geophysical Institute, Bjerknes Centre for Climate Research, University of Bergen, Bergen, Norway; [g] Nansen Environmental and Remote Sensing Center and Bjerknes Centre for Climate Research, Bergen, Norway; [h] Barcelona Supercomputing Center, Barcelona, Spain; [i] Institució Catalana de Recerca i Estudis Avançats, Barcelona, Spain; [j] Geophysical Fluid Dynamics Laboratory, Princeton, New Jersey; [k] University Corporation for Atmospheric Research, Boulder, Colorado; [l] Laboratoire d'Océanographie et du Climat, Sorbonne Université-CNRS-IRD-MNHN, Paris, France; [m] Environnements et Paléoenvironnements Océaniques et Continentaux, University of Bordeaux, CNRS, Bordeaux, France; [n] Laboratory of Numerical Modeling for Atmospheric Sciences and Geophysical Fluid Dynamics, Institute of Atmospheric Physics, Chinese Academy of Sciences, Beijing, China; [o] State Key Laboratory of Severe Weather and Institute of Tibetan Plateau Meteorology, Chinese Academy of Meteorological Sciences, Beijing, China; [p] Hadley Centre, Met Office, Exeter, United Kingdom; [q] Japan Agency for Marine-Earth Science and Technology, Yokohama, Japan; [r] Atmosphere and Ocean Research Institute, The University of Tokyo, Chiba, Japan

1. Introduction

The science of annual-to-decadal prediction aims to forecast near-term variations of climate out to 10 years or so using observationally initialized dynamical models. In recent years, it has matured from an exploratory research field into an operational service that provides annually updated multimodel forecasts under the auspices of the World Meteorological Organization (Hermanson et al. 2022).

Predictability on annual-to-decadal time scales derives from the ability to predict both internal climate variations and changes driven by external forcings, the latter becoming more important as forecast lead time increases (Boer et al. 2013). Externally forced climate predictability derives from the predictability of the responses to forcings and that of the forcings themselves. Anthropogenic greenhouse gas and aerosol forcings are predictable because emissions normally do not change substantially over a decade.[1] Solar forcings, although relatively minor, are also somewhat predictable due to the quasi-periodic nature of the solar cycle (Schurer et al. 2014).

[1] Even the relatively large temporary reductions during the COVID-19 pandemic did not detectably influence the simulated climate (Jones et al. 2021).

Unauthenticated | Downloaded 02/14/25 09:04 AM UTC

By contrast, explosive volcanic eruptions, which through associated sulfate aerosol loadings can significantly cool global surface temperatures for several years (Bethke et al. 2017), are not currently predictable.

A recent volcanic eruption having major global climatic impacts was that of Mount Pinatubo in June 1991. In this instance, global near-surface temperatures cooled by 0.2°–0.3°C (Robock and Mao 1995; Zanchettin et al. 2022), despite the long-term warming trend and an El Niño event in 1991–92 that ordinarily would have elevated global temperatures. The eruption likely affected the intensity of this El Niño (Khodri et al. 2017; Predybaylo et al. 2020), with climatic impacts on teleconnected regions. Any decadal prediction issued before this eruption would not have represented the consequent cooling and other worldwide climatic influences, rendering it essentially invalid. In addition, decadal predictions issued in years immediately following the eruption would not accurately represent its lingering impacts unless they incorporated the associated radiative effects.

Recognizing that another major eruption could occur at any time and that producers of decadal predictions should be prepared for such an eventuality, the steering group of the Decadal Climate Prediction Project (DCPP), which oversees decadal prediction activities within the World Climate Research Programme (WCRP), developed guidelines for climate forecasts after a sudden volcanic eruption.[2] This document recommends procedures for the scientific communities engaged with estimating volcanic influences on climate and producing decadal predictions to develop revised forecasts should a major eruption occur.

[2] https://www.wcrp-climate.org/images/key_deliverables/decadal_prediction/documents/Guideline_FCST_after_volcanic_erruption_DCPP_15012018.pdf.

The envisaged chain of responses is illustrated in Fig. 1. Initially, the eruption and its immediate aftermath are observed by ground-based, airborne, and orbital platforms such as the NASA/CNES *Cloud–Aerosol Lidar and Infrared Pathfinder Satellite Observations* (*CALIPSO*) satellite. Within days, crucial parameters such as the mass of sulfur dioxide (SO_2) gas injected into the stratosphere and the height profile of the injection are estimated by the WCRP's Volcanic Response (VolRes) initiative[3] through procedures like those described in Vernier et al. (2024) for the 2019 Raikoke eruption. Subsequent radiative effects are then estimated as described in the next section. Decadal prediction centers repeat their forecasts with the volcanic radiative forcings included and provide these to the WMO Lead Centre for Annual-to-Decadal Climate Prediction (LC-ADCP[4]), which issues an updated forecast.

[3] VolRes is a component of the Stratospheric Sulfur and its Role in Climate (SSiRC) activity of the APARC WCRP Core Project.

[4] http://www.wmolc-adcp.org.

This plan, while seemingly straightforward, requires significant coordination between the groups responsible for its components, as well as technical efforts by each modeling center to implement the volcanic radiative forcings and rerun the forecasts. Furthermore, unanticipated difficulties could arise when executing it for the first time. Therefore, rather than awaiting a large eruption to put the plan into action, members of the WCRP Atmospheric

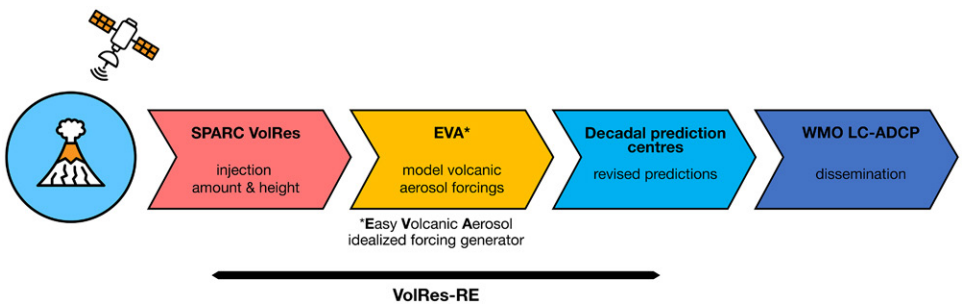

Fig. 1. Schematic of the proposed chain of responses leading to a revised annual-to-decadal prediction following a major volcanic eruption. The black arrow indicates steps encompassed by VolRes-RE.

Unauthenticated | Downloaded 02/14/25 09:04 AM UTC

Processes and Their Role in Climate (APARC) VolRes and DCPP groups and collaborators have designed and coordinated a "dry run" execution of several of its key steps, indicated by the black arrow in Fig. 1.

This effort, termed the APARC/DCPP Volcanic Response Readiness Exercise (VolRes-RE), posited the occurrence of a hypothetical large eruption in 2022 and invited international decadal prediction centers to revise their forecasts from that year incorporating associated stratospheric aerosol forcings. Specific motivations for the exercise include the following:

- Responding to a hypothetical volcanic eruption will increase the readiness of decadal prediction centers to respond to a real one.
- By working through the response process, participants may confront and remedy unanticipated issues that would delay a real response.
- The DCPP guidelines describe two possible response protocols; working through both serves to highlight their relative merits.
- Comparing modeled responses to the hypothetical eruption will highlight any major disagreements between prediction systems and motivate efforts to reconcile them.
- The VolRes-RE exercise will revise and supplement the DCPP guidelines with durable and discoverable recommendations for how the decadal prediction community should respond to a major volcanic eruption.

The remainder of this paper describes the hypothetical eruption, individual and combined responses of the participating prediction systems, and original and revised predictions as formulated by the WMO. Lessons learned and recommendations from VolRes-RE are then outlined, followed by a concluding discussion. Although the paper primarily addresses the design and preparedness aspects of VolRes-RE, this experiment also adds to previous studies of modeled climatic responses to volcanic eruptions. The simulated responses are thus examined in the last three subsections of the "process and results" section. Readers who are primarily interested in the preparedness aspects of the experiment may prefer to skip over this material. Supplementary information is provided in the appendices. Appendix A describes properties of the decadal prediction systems contributing to VolRes RE, appendix B presents the analysis methods, and appendix C shows additional results for the simulated volcanic responses.

2. The hypothetical major volcanic eruption of 2022

The hypothetical volcanic eruption that is the basis for VolRes-RE occurs in April 2022 at 17°N, a latitude similar to recent major eruptions of El Chichón (1982) and Pinatubo (1991). The stratospheric sulfur injection from this event was chosen to be 16 TgS, approximately 2 times larger than estimates of total SO_2 emission from Pinatubo (7–11.1 TgS; Guo et al. 2004) and about 4.5 times larger than from El Chichón (3.5 TgS; Carn 2022), although considerably less than from the 1815 Tambora eruption (28.1 TgS; Toohey and Sigl 2017). The interhemispheric spread of volcanic aerosols has varied for past tropical eruptions (Sato et al. 1993) with implications for the associated climate response (e.g., Haywood et al. 2013; Oman et al. 2005; Ward et al. 2021). While the spread of aerosol after Pinatubo (15°N) was balanced between the Northern and Southern Hemispheres, aerosol loading was twice as large in the NH after El Chichón (17°N) and approximately 4 times larger in the SH than in the NH after the 1963 Agung eruption (8°S). Given the relative abundance of model experiments focused on the Pinatubo eruption (e.g., Zanchettin et al. 2016) and its approximately hemispherically uniform aerosol forcing, we chose for this experiment a distribution with twice the volcanic aerosols in the Northern Hemisphere as in the Southern Hemisphere, similar to that observed for El Chichón. We note that the impacts of the Hunga eruption that occurred in January 2022 are not considered here; this eruption injected a significant amount of water vapor into the

Unauthenticated | Downloaded 02/14/25 09:04 AM UTC

stratosphere but relatively little SO_2 (Millán et al. 2022), and its net impact on climate is a topic of current research (e.g., Schoeberl et al. 2023; Jenkins et al. 2023).

Radiative forcing from volcanic aerosols spreading throughout the stratosphere following an eruption can be estimated by global atmospheric models that explicitly simulate stratospheric aerosols. However, such computations are expensive and subject to uncertainties in treatments of aerosol microphysical and transport processes (e.g., Quaglia et al. 2023). A streamlined approach is offered by the Easy Volcanic Aerosol (EVA) model family (Toohey et al. 2016; Aubry et al. 2020). EVA rapidly provides stratospheric aerosol optical properties as a function of time, latitude, height, and wavelength based on the mass of sulfur injected and the latitude and timing of the eruption. EVA output is formatted to be consistent with the stratospheric aerosol forcing of the CMIP6 historical simulations and thus is easily implemented in decadal prediction systems that employ CMIP6 models. For those systems that use CMIP5 models, a simple routine was written for this exercise to reformat the EVA output to be consistent with CMIP5 forcings. While the EVA_H tool described in Aubry et al. (2020) incorporates information on the eruption plume height and thus produces more realistic forcings for some eruptions compared to EVA, for the strong tropical eruption scenario selected for the exercise both generators produce very similar optical properties. Because early testing identified that the wavelength range produced by the web version of EVA_H[5] did not span that required by CMIP6 models, EVA was selected to provide stratospheric aerosol forcings for VolRes-RE, as suggested in the DCPP guidelines.

[5] https://volc2clim.bgs.ac.uk/.

Figure 2 compares EVA-generated forcings from the hypothetical 2022 eruption to those used for version 4 of the CMIP6 forcing based on the Global Space-Based Stratospheric Aerosol Climatology (GloSSAC) observation-based dataset (Thomason et al. 2018) from the 1991 Mount Pinatubo and the 1982 El Chichón eruptions (Luo 2018a,b). Of note is the much stronger forcing for the hypothetical 2022 event (twice as large as Pinatubo at global scales), as well as its higher initial intensity in the Northern Hemisphere, similar to that of El Chichón.

3. Process and results

a. Setup of the experiment. In September 2022, international decadal prediction centers contributing to the WMO LC-ADCP forecasts and others were invited to participate in the VolRes-RE experiment. Eight centers accepted, while others declined due to lack of resources or model incompatibility with the forcing data generated by EVA. The nine systems[6] participating in VolRes-RE are similar in number to the 10 or 11 that typically contribute to the WMO ensemble. These systems are summarized in Table A1.

[6] One participating center, CCCma, provided results from two systems.

Participants were asked to contribute, if possible, revised forecasts under two suggested procedures outlined in the guidelines, referred to here as protocols 1 and 2.

Protocol 1: Each center repeats its last forecast prior to the eruption from its original initial date, typically the preceding 1 November or 1 January, including the EVA forcing.

Protocol 2: The revised forecasts are initialized immediately before the eruption (on 1 April 2022 for VolRes-RE), and a forecast from the same date without the volcanic forcing is also run.

The volcanic response is diagnosed for each protocol by the difference between the forecasts with and without volcanic forcing. The anomaly forecast for protocol 1 (hereafter P1) which serves as a revision of the original 2022 forecast is obtained by subtracting the average of forecasts from the same initial date of many preceding years, referred to as hindcasts, as

Unauthenticated | Downloaded 02/14/25 09:04 AM UTC

described in Boer et al. (2016). Hindcasts, although expensive to produce, are essential for correcting model biases and evaluating predictive skill, so they already exist for the standard 1 November or 1 January initial dates used for P1. In the absence of hindcasts initialized on 1 April, we do not produce anomalies for protocol 2 (hereafter P2), but consider only the volcanic response. The motivation for P2 is that by initializing just before the eruption, the climate state when the eruption occurs and its influence on the response could be represented more accurately, and the response enhanced relative to the unpredictable "noise" in the forecast, which generally grows with increasing lead time.

Of the participating systems, nine contributed to P1 and seven to P2, as summarized in Table A1.

The model data requested for VolRes-RE are the same as that requested by the WMO LC-ADCP, namely monthly averages of six two-dimensional variables: near-surface air temperature, precipitation rate, and sea level pressure (priority 1); surface temperature, sea ice concentration, and Atlantic meridional overturning streamfunction (priority 2). Data spanning the initial month through the end of 2026 were required, with extensions through the end of 2031 encouraged.

Before the modified forecasts could be run, EVA-generated forcings needed to be tailored to the atmospheric grid and wavelength-dependent radiation treatments of each model. This was enabled by a version of EVA that participants could straightforwardly download from GitHub[7] and compile and run on their own systems with model-specific inputs. Outputs describing stratospheric aerosol optical properties included zonally averaged aerosol extinction, single scattering albedo, and scattering asymmetry factor as functions of latitude, height, wavelength, and time, or alternatively aerosol optical depth at 550 nm as required by some CMIP5 models.

[7] https://github.com/matthew2e/VolRes-RE-forcing.

b. Simulated volcanic response. Figure 3 shows the effect of the hypothetical volcanic forcing on global mean temperature (Figs. 3a,b) and precipitation (Figs. 3c,d) for the individual models, as well as multimodel means for the nine and seven models contributing to P1 and P2, respectively, and the six models that produced 10-yr forecasts for both P1 and P2. Vertical lines in the figure delimit posteruption cooling and recovery periods (April 2022–March 2023 and April 2023–March 2026, respectively), characterized by a rapid temperature decrease after the eruption followed by a slower decay of the volcanic influence. The maximum cooling response across individual models ranges from −0.97° to −0.57°C for P1 (from −0.93° to −0.57°C for P2), with the multimodel mean response peaking at −0.70° ± 0.14°C for P1 (−0.70° ± 0.13°C for P2) approximately 1 year after the volcanic event (uncertainty given by one standard deviation across models). The multimodel cooling response is stronger than the −0.33°C reported for the 1991 Pinatubo eruption (Zanchettin et al. 2022; Bilbao et al. 2024), consistent with the larger stratospheric sulfur injection of the hypothetical event examined here (Fig. 2). The slow recovery in the multimodel mean cooling reaches −0.28°C for P1 (−0.26°C for P2) 4 years after the event and equilibrates around zero about a decade after the eruption. The intermodel spread is broadened by the particularly strong cooling in the GFDL–SPEAR and FGOALS-f3-L, which are followed by rapid and gradual recoveries, respectively. The multimodel mean cooling of 0.44°C during the recovery phase implies that the global mean temperature during this multiyear period would be typical of that circa 2000, based on the preceding observed average rate of increase of 0.18°–0.20°C per decade from 1981 (Dunn et al. 2022).

For precipitation (Figs. 3c,d), the globally averaged multimodel mean decreases during the cooling phase by −0.07 ± 0.02 mm day^{-1} for both P1 and P2, although there are considerable temporal variability and multimodel spread. This is broadly consistent with previous

Unauthenticated | Downloaded 02/14/25 09:04 AM UTC

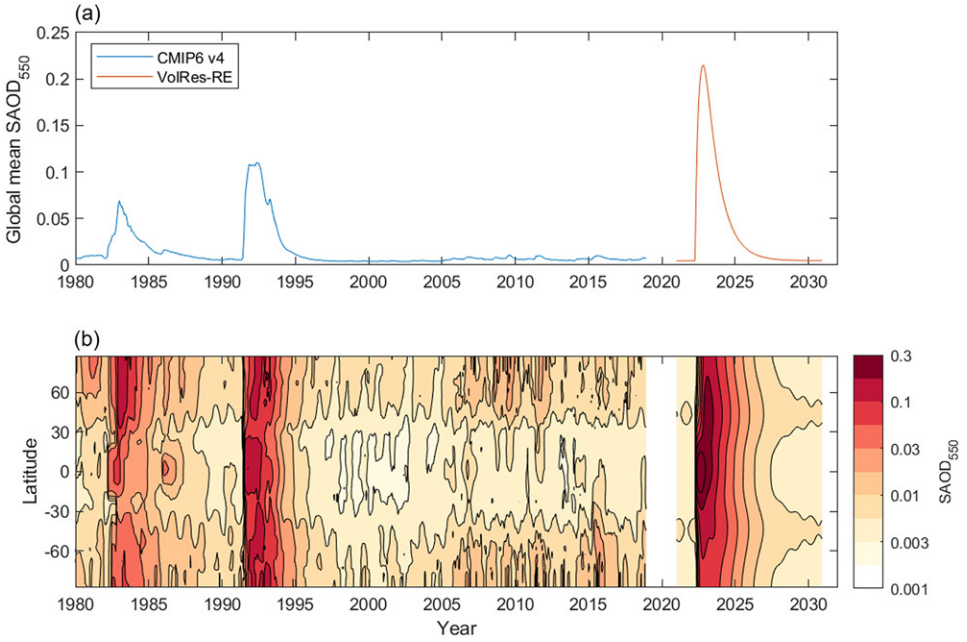

FIG. 2. (a) Global mean stratospheric aerosol optical depth (SAOD) at 550 nm from version 4 of the CMIP6 volcanic aerosol forcing dataset (1980–2018), including from the climatically impactful eruptions of El Chichón in 1982 and Mount Pinatubo in 1991 (blue) and the hypothetical VolRes-RE eruption from 2021 to 2030 (orange). (b) The same forcings as in (a), displayed in terms of zonal-mean SAOD at 550 nm as a function of time and latitude.

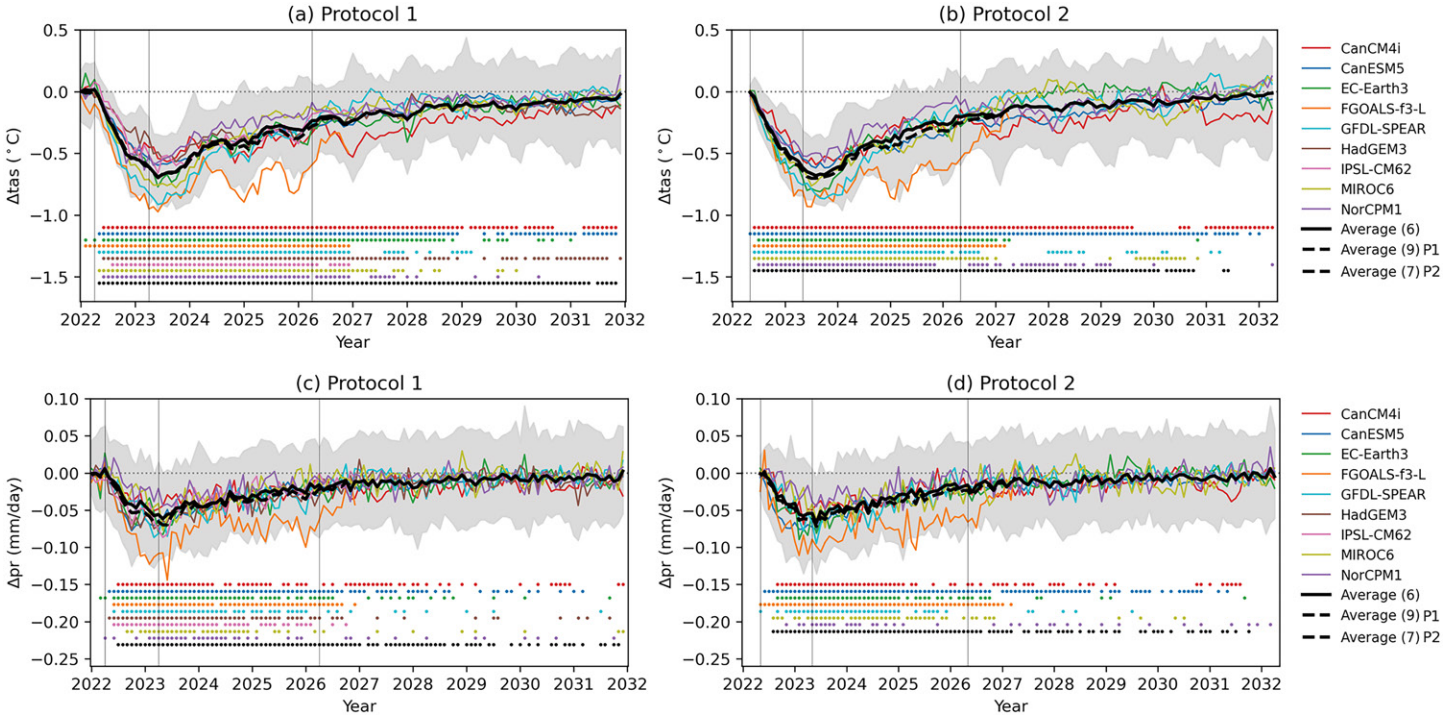

FIG. 3. Globally averaged monthly response (Volc–noVolc) of (a),(b) near-surface air temperature and (c),(d) precipitation for (a),(c) P1 and (b),(d) P2 forecasts. The symbol Δ denotes the specified quantity with volcanic forcing minus that without volcanic forcing. Individual models are shown in color. The equally weighted multimodel average for the six models having full P1/P2 forecasts is shown in solid black, and for all available models, it is shown in dashed black. Shading indicates the 5th–95th percentile ranges of the pooled ensemble for the six models having a 10-yr forecast range. Vertical lines indicate the timings of the posteruption cooling and recovery phases. Colored and black dots indicate statistically significant responses at the 95% confidence level for individual models and the six-model mean, respectively (see appendix B).

Unauthenticated | Downloaded 02/14/25 09:04 AM UTC

studies (Gu and Adler 2011; Iles et al. 2013; Iles and Hegerl 2014; Illing et al. 2018) and surpasses the −0.05 mm day^{-1} for the multimodel mean maximum response simulated for Pinatubo (Zanchettin et al. 2022). As for temperature (Figs. 3a,b), the precipitation response of FGOALS-f3-L forecasts exhibits particularly large multiannual variations, possibly linked to a strong ENSO response (next section).

The global mean response of additional climate variables is shown in Fig. C1. Of note is the contrasting intermodel response of sea level pressure, with posteruption anomalies that are positive for about half of the models and negative for the remaining models for both P1 and P2, resulting in a nonstatistically significant multimodel response. These intermodel differences deserve further analysis, as most reported dynamical responses to volcanic eruptions are local and linked to the modulation of internal modes of climate variability (e.g., Shindell 2004; Christiansen 2008; McGregor and Timmermann 2011). Arctic sea ice extent (SIE) increases after the cooling phase with the multimodel average difference peaking in October. Except for NorCPM1, the Arctic SIE response appears stronger and lasts longer for P1 than for P2. This behavior stems from the differing initialization times relative to the sea ice seasonal cycle, and the sea ice model biases, which can grow rapidly (Cruz-García et al. 2021).

Figure 4 shows the geographical distribution of the multimodel mean temperature and precipitation responses for P1. The multimodel response patterns are largely determined by the location and intensity of the volcanic eruption (Zambri and Robock 2016; Zambri et al. 2017), the resulting interhemispheric aerosol loading (Oman et al. 2005; Ward et al. 2021), and the model mean climate state at the time of the eruption (Zanchettin et al. 2012). During the cooling phase, the multimodel temperature response is strongest in the tropics and subtropics, particularly over land, and extends toward higher latitudes in North America (Fig. 4a). There is a statistically significant warming over the Greenland Sea and some warming also over Scandinavia and northern Russia that is consistent with previous studies (e.g., Hermanson et al. 2020; Azoulay et al. 2021; Bilbao et al. 2024) and has been linked to a dynamical response of the winter atmospheric circulation. The individual model responses are diverse (Fig. C2), with cooling that is strongest and most widespread for FGOALS-f3-L and GFDL–SPEAR, some warming in various high-latitude locations in all models, and a slight warming in the central tropical Pacific in HadGEM3. The variety of temperature responses likely stems from the models differing radiative and circulation responses to the volcanic forcing (Fig. C1a) as well as limited ensemble sizes (Bittner et al. 2016). The multimodel precipitation response during the cooling phase is characterized by mostly drier conditions in the tropics (Fig. 4c), particularly in the Amazon and Congo basins and the Maritime Continent. Wetter conditions occur over some subequatorial and subtropical

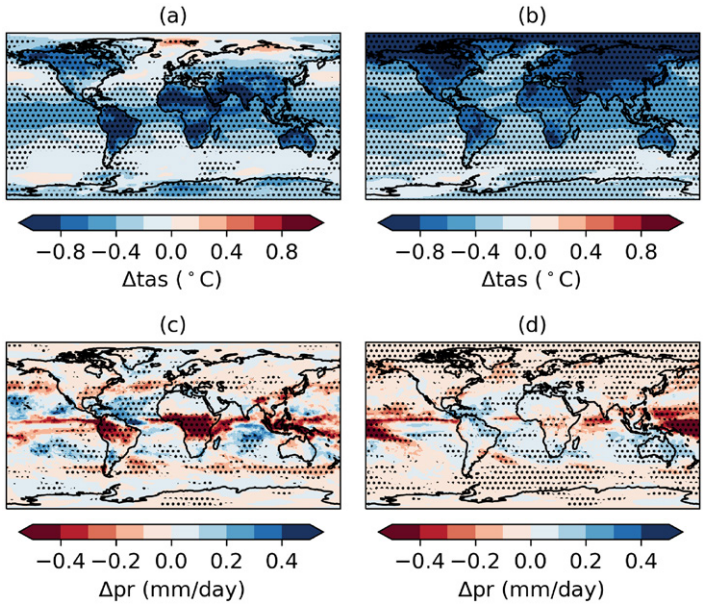

FIG. 4. Multimodel mean response (Volc–noVolc) of (a),(b) near-surface air temperature and (c),(d) precipitation forecasts averaged over the (a),(c) cooling phase (April 2022–March 2023) and (b),(d) recovery phase (April 2023–March 2026) after the volcanic eruption under P1. The symbol Δ denotes the specified quantity with volcanic forcing minus that without volcanic forcing. Stippling indicates a statistically significant response at the 95% confidence level (see appendix B).

Unauthenticated | Downloaded 02/14/25 09:04 AM UTC

ocean regions consistent with previous studies (e.g., Zuo et al. 2019; Timmreck et al. 2024), whereas the precipitation response in the extratropics is considerably weaker.

During the recovery phase, global multimodel cooling (Fig. 4b) is strongest in the Northern Hemisphere, particularly over land and in the Arctic. Individual model responses, while exhibiting some diversity, all show cooling that is stronger with more widespread statistical significance than during the cooling phase (Fig. C3). Drier conditions in the tropics are reduced over land and intensified over the western Pacific warm pool and the South Pacific convergence zone in the multimodel response (Fig. 4d). The behavior in Figs. 4c and 4d is in agreement with previous findings in which the drying effect is stronger over land and dissipates faster over land than over ocean (Illing et al. 2018); this stems from the direct impact of volcanic forcing over land and the temperature feedback over ocean (Illing et al. 2018; Iles et al. 2013).

The multimodel mean response of additional climate variables is shown in Fig. C4 for the cooling and recovery phases. During the cooling phase (Fig. C4a), the sea level pressure response has lows over the polar regions and highs over the midlatitudes, a pattern that is somewhat reversed for the composite over the recovery phase (Fig. C4b). For the Northern Hemisphere, this is consistent with the strong positive Arctic Oscillation pattern reported for the first boreal winter after the Agung and Mount Pinatubo eruptions (e.g., Stenchikov et al. 2002, 2006; Hermanson et al. 2020; Bilbao et al. 2024). Changes in atmospheric circulation and the resulting temperature response increase Arctic SIE in the decade following the eruption (Fig. C1c), most notably during the recovery period with maxima in October over the Beaufort–Chukchi–East Siberian Seas (Fig. C4d). Expanded Arctic SIE may also stem from a weaker ocean heat transport northward of 55°N in the Atlantic (Fig. C4e) and possibly the subsequent reduction in the North Atlantic SST beyond the residence time of the volcanic aerosol (Swingedouw et al. 2017). For the hypothetical eruption considered here, a strengthening of the Atlantic meridional overturning circulation (AMOC) is noticeable in the (30°–40°N, 500–2000 m) region during the cooling phase reaching up to a 0.80 Sv ($1\ \text{Sv} \equiv 10^6\ \text{m}^3\ \text{s}^{-1}$) increase (Fig. C4e) and in the (10°–30°N, 1000–2000 m) and (40°–55°N, 1000–2000 m) regions during the recovery phase reaching up to 0.23 and 0.38 Sv increases, respectively (Fig. C4f), consistent with Mignot et al. (2011).

The multimodel temperature response patterns are broadly similar between P1 and P2 (Fig. C5), particularly over the tropics, but there are some differences. In particular, there is a relatively strong cooling over western Canada and Alaska for P1 during the first posteruption year that is not present for P2, and there is notable warming over North Eurasia and the Barents–Kara Seas for P2 that is weaker and more localized around the Greenland Sea for P1 (Figs. C5a,b). Warming over Eurasia after the Agung, El Chichón, and Pinatubo events (Robock and Mao 1992) was reproduced with climate models (Zambri and Robock 2016; Paik et al. 2023; Bilbao et al. 2024), although they appear weaker and confined to smaller areas than in observations (Zambri and Robock 2016; Hermanson et al. 2020). The stronger and more widespread warming for P2 than for P1 may be an indication that this signal is relatively weak compared to internal variability (DallaSanta and Polvani 2022), and it is better represented for the forecast initialized closer to the volcanic event. A posteruption warming over these regions may be favored by the negative phase of the Pacific decadal oscillation (Illing et al. 2018), as was the case for the Agung event (Bilbao et al. 2024) and the hypothetical eruption examined here. During the recovery phase, the cooling responses are largely similar between P1 and P2 (Figs. C5c,d). For precipitation (Fig. C6), the response patterns are largely similar for both protocols, with the exception of a drying response during the recovery phase that is weaker in the western tropical Pacific, and stronger in the central and eastern tropical Pacific, in P2 as compared to P1 (Figs. C6c,d).

Unauthenticated | Downloaded 02/14/25 09:04 AM UTC

c. 2023 El Niño. A notable aspect of the predictions examined here is the presence of El Niño–like conditions during their second full year, 2023. This is evident in the predicted multimodel annual mean near-surface air temperature anomalies for 2023 in the unperturbed case (Figs. 5a and C7 for the individual models) and with volcanic forcing (Figs. 5b and C8 for the individual models), which both exhibit a pronounced El Niño–like warming in the central and eastern equatorial Pacific. These predictions agree with the observed major El Niño event that emerged from a preceding 3-yr La Niña in the first half of 2023. The fact that these P1 predictions were initialized from late 2021 to the beginning of 2022 and show broadly similar ENSO behavior to the late-2022-initialized 2023 forecast issued by the LC-ADCP (WMO 2023) suggests that the peak of this El Niño in late 2023 may have been predicted 2 years or more in advance.

This result bears on two scientific issues. The first is the extent to which El Niño and La Niña are predictable on multiyear time scales. Previous studies have indicated that at least some El Niño and La Niña events (principally the latter) can be predicted by multiyear-to-decadal forecast systems up to 2 years or more in advance (Gonzalez and Goddard 2016; DiNezio et al. 2017). Successful prediction of the 2023–24 El Niño event on such time scales would be especially noteworthy because La Niña-to-El Niño transitions have historically been less predictable than more common El Niño-to-La Niña transitions (Sharmila et al. 2023). However, the models did not predict the observed persistence of La Niña throughout 2022 before El Niño onset.

The second scientific issue is the influence of major volcanic eruptions on ENSO, including the possibility that El Niño conditions such as those that occurred following the El Chichón and Pinatubo eruptions can be induced, or at least intensified, by a volcanic event (Dogar et al. 2023). To address these two issues, Figs. 5c and 5d show the relative Niño-3.4 index for the individual models and the multimodel average with and without volcanic forcing. This index is defined following Khodri et al. (2017) and van Oldenborgh et al. (2021) as

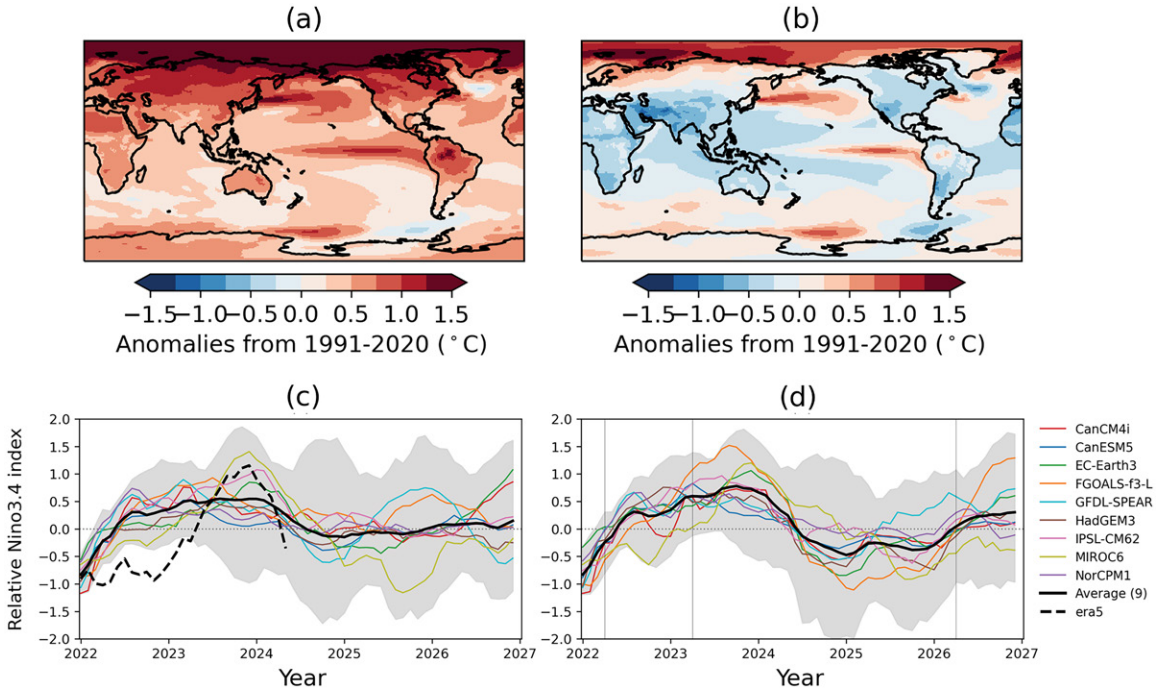

Fig. 5. (a),(b) Multimodel mean predictions of 2023 annual mean anomalies from the 1991 to 2020 average for near-surface air temperature under P1 (a) noVolc and (b) Volc; (c),(d) monthly relative Niño-3.4 index predictions under P1 (c) noVolc and (d) Volc. Colors in (c) and (d) indicate individual models, and black curves indicate the equally weighted multimodel average. Shading indicates the 5th–95th percentile range of the pooled ensemble. The dashed curve in (c) represents values from ERA5 (Hersbach et al. 2020; the last month shown is May 2024). Vertical lines in (d) indicate the timings of the posteruption cooling and recovery phases.

Unauthenticated | Downloaded 02/14/25 09:04 AM UTC

the difference between the SST anomaly in the Niño-3.4 region and that averaged over the 20°S–20°N oceans, in order to isolate the ENSO signal from the long-term warming trend and the posteruption cooling.

For the forecast with volcanic forcing (Fig. 5d), the multimodel relative Niño-3.4 anomalies are positive from June 2022 to 2024 and larger than in the unperturbed case (Fig. 5c), peaking at 0.83°C in October 2023. The warm increase is statistically significant in the second year after the eruption (Fig. C9), which is consistent with the ENSO response to low-latitude explosive volcanic events in April during neutral or El Niño–like conditions (Predybaylo et al. 2020). Mechanisms underlying this behavior have been proposed, including the land–ocean temperature gradient, the ocean-dynamical thermostat, or shifts in the intertropical convergence zone (Khodri et al. 2017; Miao et al. 2018; Zuo et al. 2018; Pausata et al. 2020; McGregor et al. 2020). These can weaken the easterly trade winds or trigger anomalous westerly winds favoring or enhancing El Niño–like conditions through the Bjerknes feedback. Such behavior is consistent with the reduced precipitation over the Maritime Continent (Zuo et al. 2018) during the cooling phase (Fig. 4c) as well as the drier conditions in tropical America and Africa (Khodri et al. 2017). The subsequent negative anomalies of the multimodel relative Niño-3.4 index after mid-2024 (Figs. 5c,d) are enhanced by the volcanic forcing, although there is considerable intermodel spread (Fig. C9). The strengthening of the negative anomalies is in accord with previous work showing an increased probability of La Niña–like conditions following El Niño response 3–4 years after the eruption (Adams et al. 2003; Maher et al. 2015; Zuo et al. 2018; Bilbao et al. 2024).

While ENSO is affected by the location (e.g., Pausata et al. 2015, 2016; Zuo et al. 2018; Sun et al. 2019; McGregor et al. 2020) and strength (e.g., Ohba et al. 2013; McGregor and Timmermann 2011) of volcanic eruptions, it is sensitive also to the climate conditions preceding the events and the timing of the eruptions relative to the seasonal cycle (Predybaylo et al. 2017, 2020; Zuo et al. 2021). The strength and low-latitude location of the eruption may have favored an ENSO response, but the timing and background climate conditions may not have. The volcanic event occurs in early spring, when wind-related noise and a coupled atmosphere–ocean instability (Samelson and Tziperman 2001) can enhance mixing and heat exchange dampening the impact of the eruption on ENSO, and during La Niña–like or near-neutral conditions, for which the ENSO response to volcanic eruptions is weakest (Predybaylo et al. 2017, 2020). The timing and climate conditions preceding the eruption may thus have prevented a stronger ENSO response compared to a similar volcanic event occurring during summer or fall and/or preceded by El Niño–like conditions.

In summary, Figs. 5c, 5d, and C9 indicate that the volcanic eruption does not modify the timing of El Niño onset or the duration of El Niño–like conditions. The volcanic eruption does enhance the positive anomalies of the relative Niño-3.4 index by up to 0.25°C (Fig. C9) 1–2 years after the event consistent with Hermanson et al. (2020), leading to a potentially stronger 2023/24 El Niño relative to the original forecast. There is also a tendency for enhanced La Niña–like conditions afterward. However, the responses of the individual models vary, with CanESM5 showing one of the weakest responses and FGOALS-f3-L the strongest, particularly during the recovery phase (Fig. C9).

d. Implied revision to 2022 annual-to-decadal climate prediction. Figures 6a, 6c, and 6e show the multimodel year 1–5 (2022–26) annual mean anomaly forecasts for temperature, precipitation, and sea level pressure relative to the 1991–2020 average as would have been issued in early 2022. We follow closely the format of the WMO LC-ADCP (WMO 2022, 2023) but emphasize that the model ensemble for these two activities is different. Thus, the anomaly maps shown here differ slightly from the LC-ADCP versions. Figures 6b, 6d, and 6f show the P1 revised forecasts influenced by the hypothetical volcanic eruption.

Unauthenticated | Downloaded 02/14/25 09:04 AM UTC

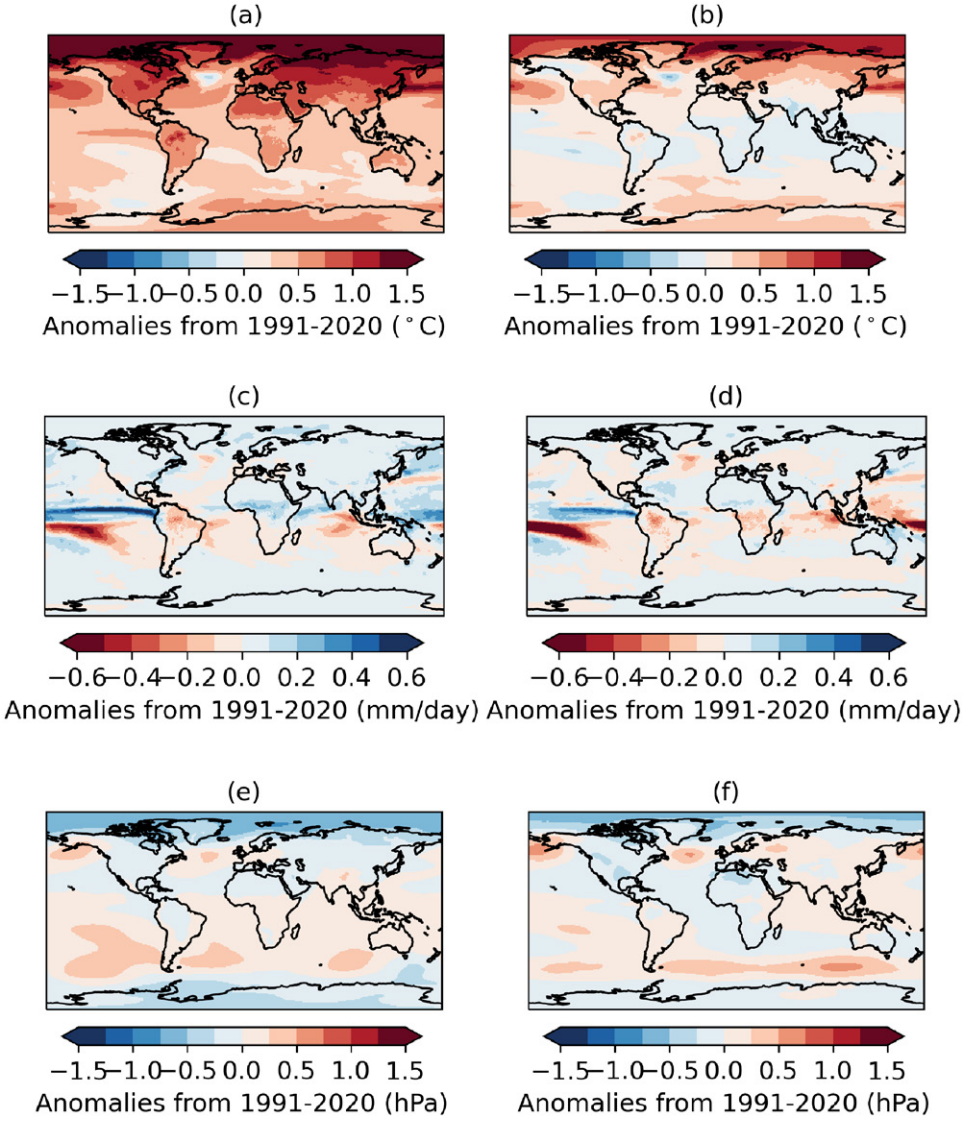

FIG. 6. Multimodel mean predictions for 2022–26 annual mean anomalies from the 1991 to 2020 average for (a),(b) near-surface air temperature, (c),(d) precipitation, and (e),(f) sea level pressure under P1 (a),(c),(e) noVolc and (b),(d),(f) Volc. The noVolc forecasts are analogous to the LC-ADCP 2022-issued forecasts, except that the model ensemble is different.

The corresponding extended boreal summer (May–September) and winter (November–March) multiyear forecasts with and without volcanic forcing, as well as the volcanic response, are shown in Figs. C10–C12.

Without volcanic forcing, the annual mean temperature forecast is higher than the 1991–2020 average nearly everywhere, particularly over high-latitude Northern Hemisphere land and the Arctic Ocean (Fig. 6a), reflecting the rapid global temperature increase over the past several decades (Gulev et al. 2021). The enhanced Arctic warming is stronger during November–March (Fig. C10b) than during May–September (Fig. C10a). The revised forecast displays cool anomalies rather than warm anomalies throughout much of the tropics and subtropics, as well as northwestern North America (Fig. 6b). While the Arctic warming is much reduced in the revised forecast, warm anomalies over the Greenland–Barents–Kara Seas remain high. Posteruption cooling is strongest over land and in the Arctic (Figs. C10e,f), most notably from November to March (Fig. C10f).

For precipitation, the original 2022–26 forecast predicts widespread wet anomalies in the Northern Hemisphere and dry anomalies over the southern tropics and extratropics

Unauthenticated | Downloaded 02/14/25 09:04 AM UTC

(Fig. 6c). The volcanically perturbed forecast is drier in both hemispheres (Fig. 6d), with wet anomalies in the unperturbed forecast shifting to dry anomalies in the Congo basin and far western tropical Pacific. Those changes are evident in both May–September and November–March (Fig. C11), with the dry anomalies over Africa and the Indian Ocean shifting southward in boreal winter, when dry anomalies also prevail along the Pacific and Atlantic storm tracks (Fig. C11f).

The volcanic eruption appears to cause predicted sea level pressure anomalies to reverse sign over much of Eurasia (Figs. 6e,f). In addition, low pressure anomalies over the northern and southern polar regions are diminished, primarily in boreal summer (Figs. C12a,c,e), and subpolar high pressure anomalies generally strengthen, primarily in the extended winter season of each hemisphere.

Overall, the differences between the original and revised forecasts are sufficiently large that the hypothesized eruption would have substantially reduced the value of the original forecast for decision-making. This is especially true for not only temperature but also precipitation. In a case such as this, issuance of a revised forecast using the methods described here is clearly justified. In the event of a real eruption, a decision on whether to revise the forecast would begin with advice from the APARC VolRes group as to whether the eruption is likely to be climatically significant. If significant cooling is a possibility, then estimates of the volcanic forcing would be generated as described above and provided to modeling centers that contributed to that year's LC-ADCP forecast. After revised forecasts are received, the LC-ADCP would decide whether to update the current forecast based on whether the volcanically induced changes are statistically significant or otherwise obviously modify the forecast.

4. Lessons learned and recommendations

A primary motivation of VolRes-RE has been for decadal prediction centers to gain experience incorporating the type of rapidly developed, flexibly configured volcanic forcing data that would be provided in the event of an actual large eruption. This was not a trivial exercise, in part because the groups that develop decadal prediction systems and produce forecasts are often separate from those that develop the atmospheric components of the models and have the greatest knowledge of and experience with treatments of stratospheric aerosols. Fortunately, the participating groups were able to enlist the required expertise to implement the EVA-generated forcings. Nonetheless, this disconnect could be a barrier for decadal prediction producers who use models developed at other centers.

Another purpose of VolRes-RE was to confront and remedy technical and other issues that would have delayed an actual response. Several such issues relating to obtaining and ingesting the volcanic forcing were identified by beta testers from BCCR, BSC, and CCCma (Table A1). For example, minor issues with spatial and temporal dimensioning and the length of the time series were quickly remedied by the beta testers before releasing the EVA package to all participating groups.

After the final EVA package was distributed and the revised forecasts were produced, several errors were found that required time to identify and correct. This was not surprising, considering this was the first time the response procedures had been carried out by the participants. For example, protocol 2 data provided by one center initially was missing outputs extending from the April 2022 initialization month to the November 2022 initialization of the next year's forecast, and another center mistakenly employed forcing from a weaker historical event in their initial revised forecasts. In addition, the forecast data received in some cases deviated from formatting standards requested by the WMO, which led to data processing delays. Awareness of these issues obtained through participation in VolRes-RE should reduce avoidable delays when a real response is needed.

Unauthenticated | Downloaded 02/14/25 09:04 AM UTC

Experience gained from VolRes-RE has informed the following recommendations:

- Several invited groups were unable to participate, either because they lacked the human and/or computing resources required or because the treatment of stratospheric aerosols in their model was not compatible with forcings from EVA. Such groups who wish to revise their forecasts when an actual eruption occurs should develop a plan for the necessary responses.
- If some of the systems that originally contributed to the WMO forecast in the year of the eruption are unable to revise their forecasts, then the revised WMO forecast products should be based on the subset of systems that updated their forecasts to include volcanic forcings.
- Similarly, forecasts produced in years following the eruption while its climatic impacts are expected to remain significant should be based on systems that include the volcanic forcings.
- As EVA tools are updated in the future, it will be important to maintain infrastructure to enable rapid production of forcing fields in the aftermath of eruptions by automated and easily accessed means, such as publicly available code and/or web forms.
- If an eruption occurs late in the calendar year, then effort should be focused on incorporating volcanic radiative effects into the next year's forecast, rather than revising the forecast from the current year.
- Finally, although protocol 2 provides an interesting comparison, a real response should follow protocol 1, given that the protocol 1 and 2 volcanic responses exhibited only relatively minor regional differences. Protocol 1 is simpler to implement since it requires running one forecast rather than two new forecasts and does not require preparing initial conditions on a different date than the original forecast. Decadal prediction centers can thus respond more rapidly using protocol 1. In addition, protocol 1 forecasts are simpler to interpret because the revised raw forecasts can simply be differenced with existing hindcast climatologies to produce revised forecast anomalies, whereas protocol 2 produces a correction to the original forecast that either must be presented separately or else added to the original forecast which would be inconsistent from a modeling perspective. Finally, any potential advantages of protocol 2 are expected to increase as an eruption occurs later in the calendar year, whereas the utility of the revised forecast diminishes later in the calendar year (compare previous recommendation).

5. Conclusions and outlook

The main objectives of VolRes-RE were to increase the readiness of the decadal prediction community to respond to a major volcanic eruption, identify and resolve "sticking points" in this process, and provide recommendations for and durable documentation of the response procedures. As described in this paper, these objectives have largely been met. Based on the experience gained, when a major eruption occurs, a prepared scientific community should be able to provide estimates of volcanic forcings to decadal prediction centers within a few days, revise the individual forecasts within 2 weeks or so, and disseminate a consolidated revised forecast within about another week. Therefore, it should be possible to complete the chain of responses illustrated in Fig. 1 within about 1 month.

The accuracy of decadal predictions revised after future volcanic eruptions will depend strongly on the accuracy of the aerosol forcings used. Forcings from EVA, which are constrained by satellite observations of the aerosol from Pinatubo, have been found to be within the relatively large range simulated by prognostic aerosol models (e.g., Clyne et al. 2021) and produce global mean temperature anomalies consistent with proxy records for large eruptions of the last millennium when uncertainties in forcings are considered (Lücke et al. 2023). However, if the aerosol from a future eruption behaves significantly differently from that of

Unauthenticated | Downloaded 02/14/25 09:04 AM UTC

Pinatubo, EVA forcing predictions may be inaccurate. Using models that include prognostic treatments of stratospheric aerosols and their radiative effects may offer advantages over the prescribed forcing from EVA, but they have their own limitations (e.g., Quaglia et al. 2023) and are also highly sensitive to uncertainties in the estimated SO_2 injection and its vertical profile. Therefore, irrespective of the method used to estimate the aerosol forcing after future eruptions, decadal predictions might require more than one revision: Following the initial revision based on SO_2 injection amounts estimated in the first days after the eruption, a further updated prediction could be released based on forcing fields constrained by aerosol extinction measured by satellite sensors. In the case of a close succession of major volcanic eruptions (Zanchettin et al. 2016), additional revisions may be required. Future volcanic response protocols might also include direct volcanic injection of stratospheric water vapor, as observed in the 2022 Hunga eruption, to account for its surface warming effect (Millán et al. 2022; Jenkins et al. 2023; Schoeberl et al. 2023). Current work on simulating the combined effects of the water vapor and sulfate aerosol from the Hunga eruption (e.g., Zhu et al. 2022) will guide consideration of representing their joint influences in future decadal predictions.

In addition to the objectives mentioned above, VolRes-RE provides a measure of additional value to the community that studies and models climatic responses to volcanic eruptions. While the event considered is hypothetical, so the simulated responses cannot be compared with observations, the fact that it is considerably stronger than any in the recent observational record provides both a potential "stress test" for the behavior of models under very strong volcanic forcing and simulations of how such an extreme event may affect present-day climate. The fact that the simulated eruption occurs under relatively constrained climatic conditions due to model initialization < 6 months beforehand may offer a useful supplementary perspective to previous experiments that have aimed to carefully intercompare volcanic responses between models (Zanchettin et al. 2019, 2022). Although there are no extreme outliers among the volcanic responses examined here, they do exhibit a larger diversity than in the especially carefully controlled experiment of Zanchettin et al. (2022) that considered a different set of models, each providing 25 ensemble members. This motivates efforts to understand the origins of the differences seen here.

The surprising result that every system simulates El Niño conditions in 2023 following initialization 1–2 years earlier bears on the multiyear predictability of El Niño and La Niña events (Gonzalez and Goddard 2016), potential windows of opportunity when initializing predictions in ENSO peak phases (Liu et al. 2023), and the utility of multiyear dynamical predictions (Yeager et al. 2022). That El Niño conditions occurred both with and without volcanic forcing adds to previous modeling studies that examined conditions under which large volcanic events could trigger El Niño onset (Khodri et al. 2017; Predybaylo et al. 2017).

Data provided currently to the WMO LC-ADCP consist of monthly averages for a few key climate variables. However, as the capacities of the LC-ADCP and its contributors develop further, it will become desirable to provide higher-frequency model outputs. Following an eruption, such data will enable predicted impacts on probabilities of extreme climate events to be assessed. Such information would be of value because major eruptions are known to favor severe droughts and winter cold surges while diminishing the probability of heat waves and flooding (e.g., Paik and Min 2018; Wang et al. 2021; Paik et al. 2022; Freychet et al. 2023).

Annual-to-decadal predictions have recently become a WMO service and are increasingly informing sectoral decision-making worldwide (Dunstone et al. 2022; O'Kane et al. 2023). Thus, it is more important than ever that the decadal prediction community be able to respond to the occurrence of a major volcanic eruption in order to represent its impacts on predicted near-term climate. By undertaking a simulated response involving international decadal prediction centers, the exercise described here has increased readiness for that eventuality.

Unauthenticated | Downloaded 02/14/25 09:04 AM UTC

Acknowledgments. C. T. is funded by the German Research Foundation (DFG), research unit FOR 2820 VolImpact (Grant 398006378). L. H. and D. S. were supported by the Met Office Hadley Centre Climate Programme funded by BEIS and Defra and by the EUCP project funded by the European Commission's Horizon 2020 Programme, Grant Agreement 776613. I. B. is funded by the Research Council of Norway (Grant 309562; Climate Futures). Y. W. is funded by the Trond Mohn Foundation under Project BFS2018TMT01. H. T. and T. K. were supported by the MEXT program for the advanced studies of climate change projection (SENTAN) Grant JPMXD0722680395.

Data availability statement. P1 and P2 forecasts are available at https://crd-data-donnees-rdc.ec.gc.ca/CCCMA/products/VolRes-RE and will be durably accessible via https://open.canada.ca/data/dataset/ under the search term "VolRes-RE." P1 hindcasts are available from the WMO LC-ADCP or directly from the producing centers upon request. Monthly surface temperatures from ERA5 used to compute the observation-based relative Nino-3.4 index are available through the Copernicus Data Store at https://cds.climate.copernicus.eu/.

APPENDIX A
Participating Decadal Prediction Systems

Table A1 describes properties of the decadal prediction systems contributing to VolRes-RE.

Table A1. Properties of the decadal prediction systems contributing to VolRes-RE, including (from left to right) the model name and originating modeling center; spatial resolution of the atmosphere and ocean components; month at the beginning of which the P1 forecasts are initialized (either November 2021 or January 2022); whether participants provided a P2 forecast; the number of full years in the P1 and P2 forecasts; ensemble size of the associated hindcasts and provided forecasts; initialization technique applied to the atmosphere (A), ocean (O), and/or SST: "Full" if actual values of observation-based fields are used and "Anom" if observed anomalies superimposed on the model climatology; and references containing further information about each system. Systems with an asterisk (*) next to the model name contributed to the WMO LC-ADCP forecast for 2022–26. The participating centers are CCCma: Canadian Centre for Climate Modelling and Analysis; BSC: Barcelona Supercomputing Centre; LASG: The State Key Laboratory of Numerical Modeling for Atmospheric Sciences and Geophysical Fluid Dynamics; GFDL: Geophysical Fluid Dynamics Laboratory; MOHC: Met Office Hadley Centre; IPSL: Institute Pierre-Simon Laplace; JAMSTEC/UT/NIES: Japan Agency for Marine-Earth Science and Technology/University of Tokyo/National Institute for Environmental Studies; BCCR: Bjerknes Centre for Climate Research.

Model (center)	Resolution (A: atm; O: ocean)	P1 init mon	P2 fcst	Fcst range P1/P2 (yrs)	Ens size hind/fcst	Init	Ref
CanCM4i* (CCCma)	A: T63L35 O: 1.4° × 0.9°L40	Jan	Yes	10/10	10/10	A: Full O: Full	Merryfield et al. (2013)
CanESM5 (CCCma)	A: T63L49 O: 1° × 1°L45	Jan	Yes	10/10	20/40	A: Full O: Full	Sospedra-Alfonso et al. (2021)
EC-EARTH* (BSC)	A: T255L91 O: 1° × 1°L75	Nov	Yes	10/10	10/10	A: Full O: Full	Bilbao et al. (2021)
FGOALS-f3-L* (LASG)	A: 100-km L32 O: Tripolar L31	Nov	Yes	9/5	9/9	A: None O: Anom	Wu et al. (2018), Hu et al. (2023)
SPEAR (GFDL)	A: 100-km L33 O: 1° × 1°L75	Jan	Yes	10/10	10/10	A: Full SST: Full	Yang et al. (2021)
HadGEM3* (MOHC)	A: N216L85 O: 0.25° × 0.25°L75	Nov	No	10/—	10/10	A: Full O: Full	Sellar et al. (2020)
CM62-ESMCO2 (IPSL)	A: 1.25° × 2.5° × L79 O: 1°L75	Jan	No	5/—	5/10	A: None O: Anom	Estella-Perez et al. (2020)
MIROC6* (JAMSTEC/UT/NIES)	A: T85L81 O: 1° × 1°L62	Nov	Yes	10/10	10/10	A: Full O: Anom	Kataoka et al. (2020)
NorCPM1* (BCCR)	A: 1.9° × 2.5°L26 O: 1° × 1°L53	Nov	Yes	10/10	10/30	A: None O: Anom	Bethke et al. (2021)

Unauthenticated | Downloaded 02/14/25 09:04 AM UTC

APPENDIX B
Analysis Methods

Multimodel means are computed as the average of ensemble means across models. For each model, statistical significance is computed as follows. The M pairs of perturbed and unperturbed ensemble members (with M equal to the model ensemble size) are chosen at random with replacement to provide M differences quantifying volcanic response. The ensemble mean of these M differences is taken. This process is repeated 1000 times to build the bootstrapping sampling distribution of the ensemble mean difference. The 2.5th–97.5th percentile of this distribution gives a 95% confidence interval. If this confidence interval does not cross zero, we conclude that there is a volcanic response at the 95% confidence level. For the multimodel mean, we implement the same procedure except that the ensemble mean of individual models is used instead of the pooled ensemble. This guarantees that all models are weighted equally.

Climatology to compute P1 forecast anomalies is taken as the average hindcast for a given target month, with the average taken over the 1991–2020 target period. The resulting lead month-dependent climatology is subtracted from the forecasts to produce the anomalies. Hindcasts initialized on 1 April were not requested, as only perturbed minus unperturbed forecast differences are considered for P2. Globally averaged anomalies are area weighted, and sea ice extent anomalies are computed without normalization by the total area. Sea ice extent is the total area of grid cells having ice concentration ≥ 15%.

Unauthenticated | Downloaded 02/14/25 09:04 AM UTC

APPENDIX C

Supplementary Figures

Figures C1–C12 show additional results for the simulated volcanic responses of individual models and the multimodel average, annual and multiannual predictions with and without volcanic forcing, and results for additional variables requested by the LC-ADCP.

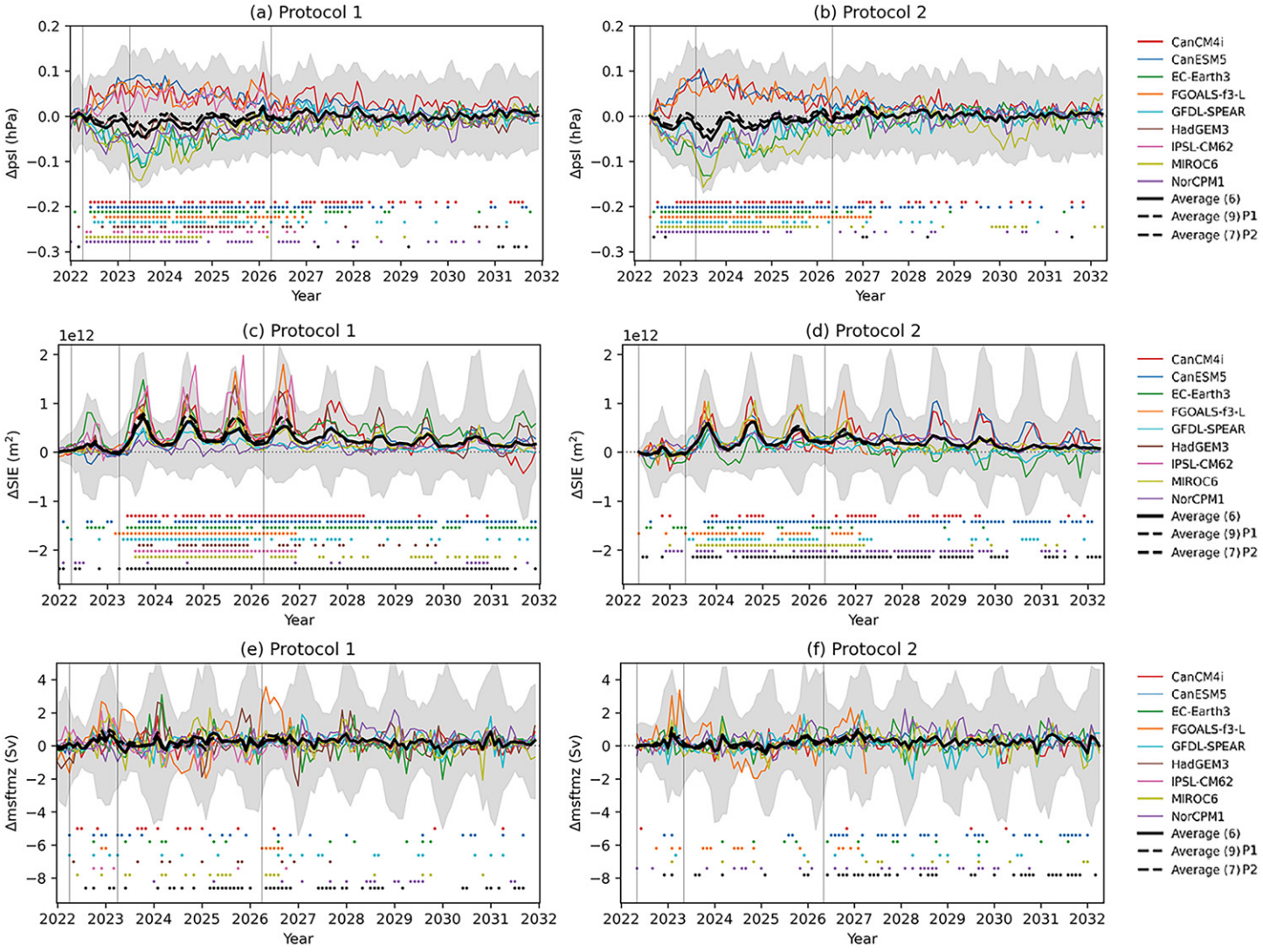

FIG. C1. As in Fig. 3, but for (a),(b) globally averaged sea level pressure, (c),(d) Arctic SIE (defined as the total area for which Arctic sea ice concentration exceeds 15%), and (e),(f) Atlantic overturning streamfunction averaged over (30°–50°N, 1000–2000 m). Color and black dots indicate statistically significant responses at the 95% confidence level for individual models and the six-model mean, respectively (see appendix B).

Unauthenticated | Downloaded 02/14/25 09:04 AM UTC

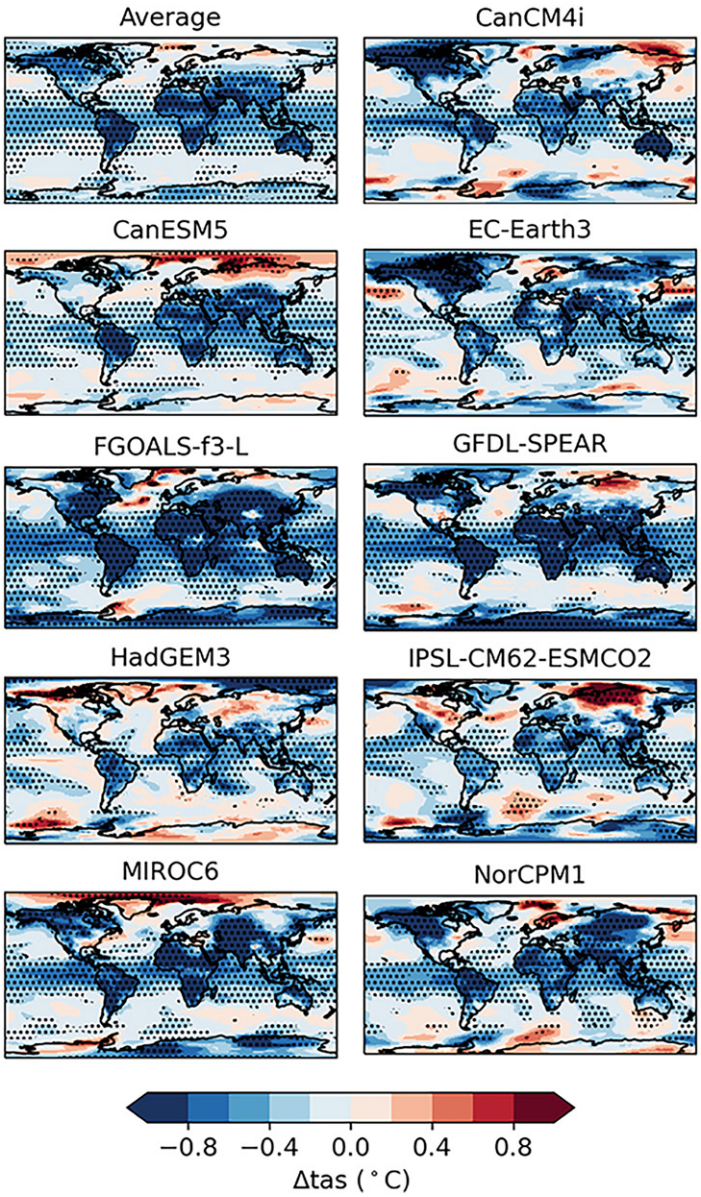

FIG. C2. Near-surface air temperature response during the cooling phase for the individual models. The symbol Δ denotes the difference in the specified quantity with and without volcanic forcing. The multimodel average response is also shown in Fig. 4a. Stippling indicates a statistically significant response at the 95% confidence level (see appendix B).

Unauthenticated | Downloaded 02/14/25 09:04 AM UTC

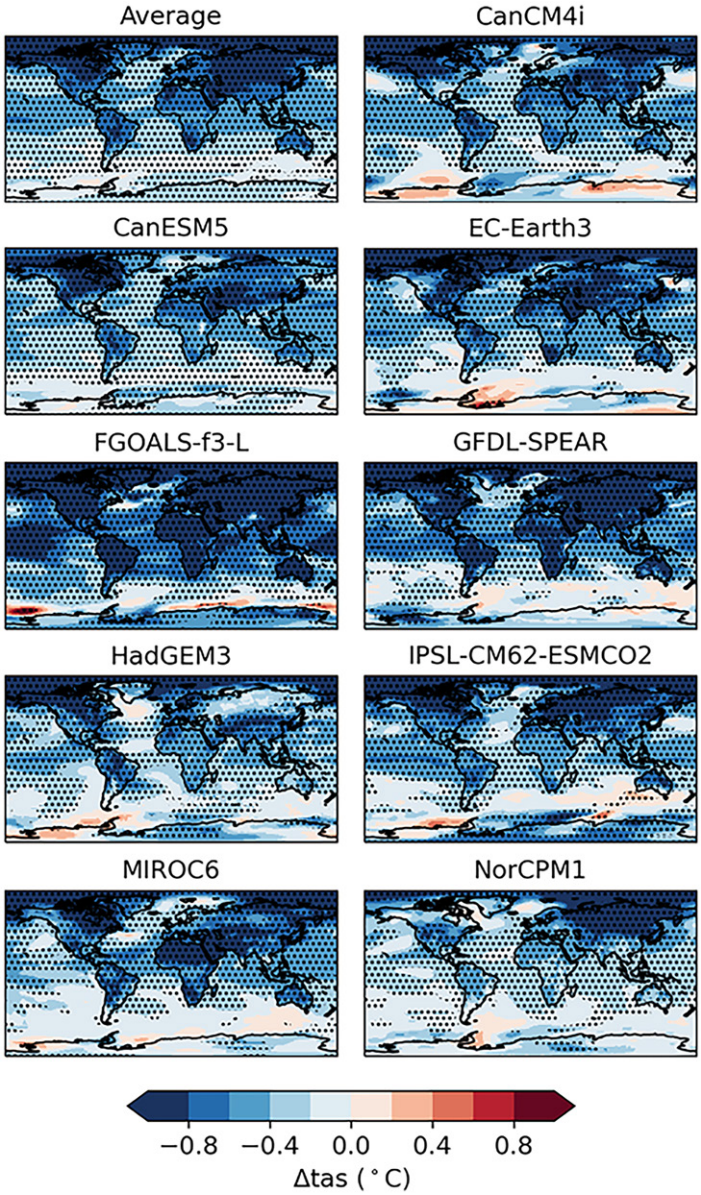

FIG. C3. Near-surface air temperature response during the recovery phase for the individual models. The symbol Δ denotes the difference in the specified quantity with and without volcanic forcing. The multimodel average response is also shown in Fig. 4b. Stippling indicates a statistically significant response at the 95% confidence level (see appendix B).

Unauthenticated | Downloaded 02/14/25 09:04 AM UTC

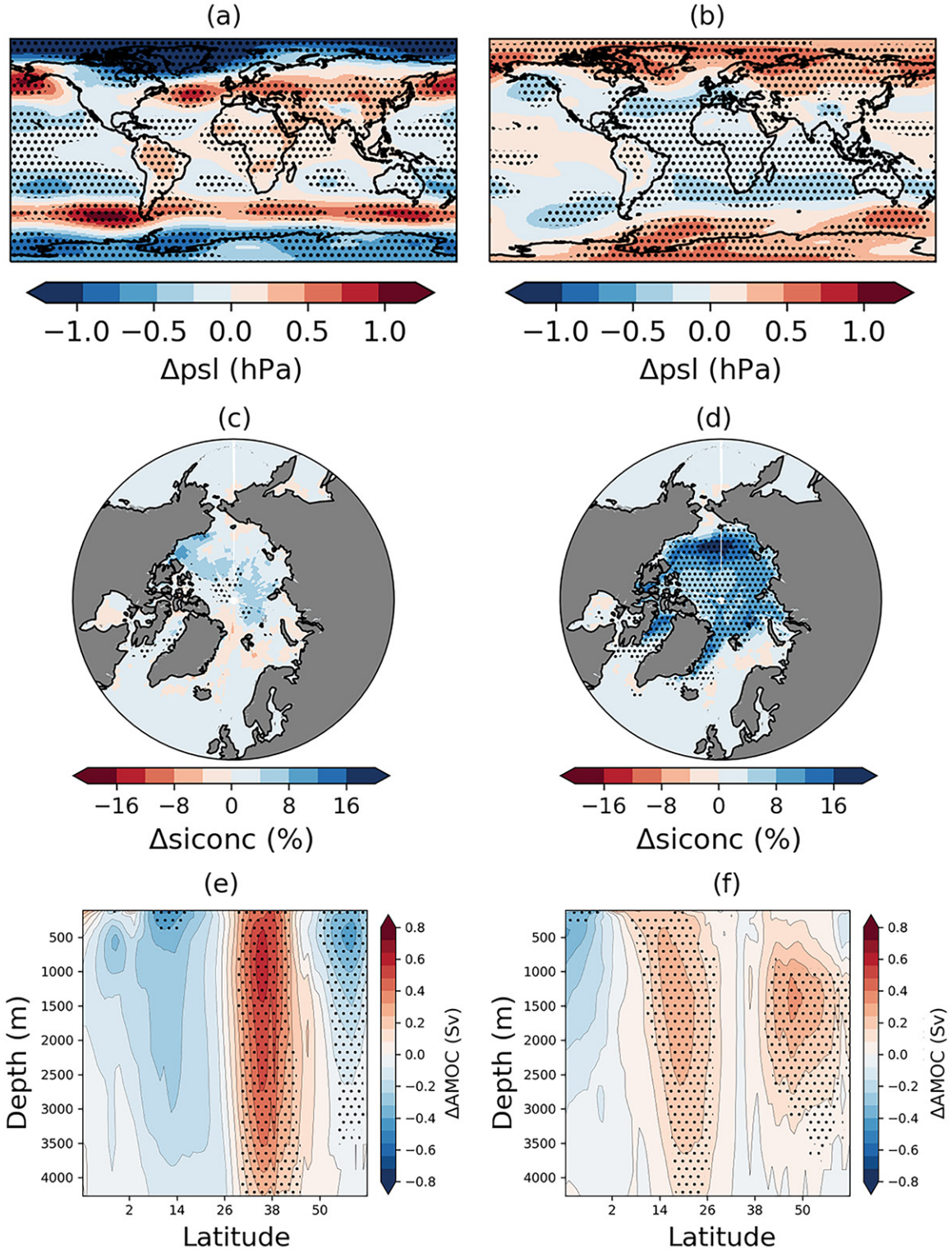

FIG. C4. As in Fig. 4, but for (a),(b) sea level pressure, (c),(d) Arctic sea ice concentration, and (e),(f) AMOC. Stippling indicates a statistically significant response at the 95% confidence level (see appendix B). October sea ice concentration averages are shown for (c) and (d).

Unauthenticated | Downloaded 02/14/25 09:04 AM UTC

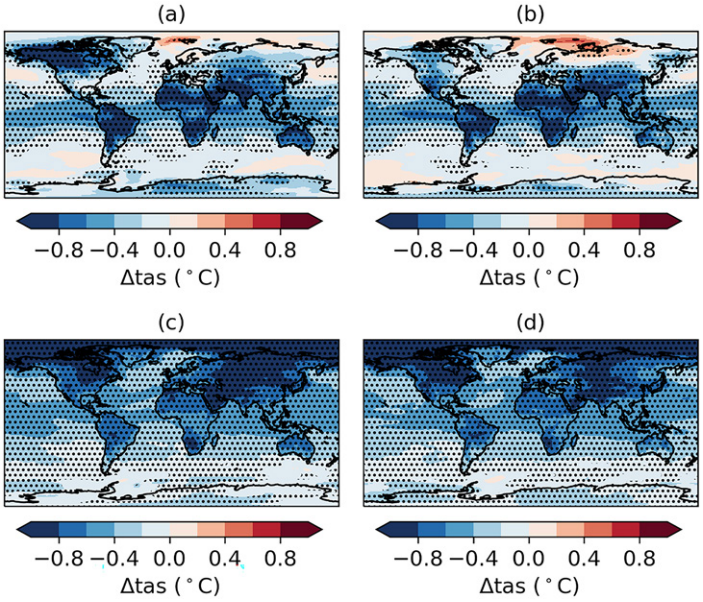

FIG. C5. Multimodel mean response (Volc–noVolc) of near-surface air temperature (a),(c) P1 and (b),(d) P2 forecasts averaged over the (a),(b) cooling phase (April 2022–March 2023) and (c),(d) recovery phase (April 2023–March 2026) after the volcanic eruption. The symbol Δ denotes the difference in the specified quantity with and without volcanic forcing. The multimodel average is over the six models having full P1/P2 forecasts. Stippling indicates a statistically significant response at the 95% confidence level (see appendix B).

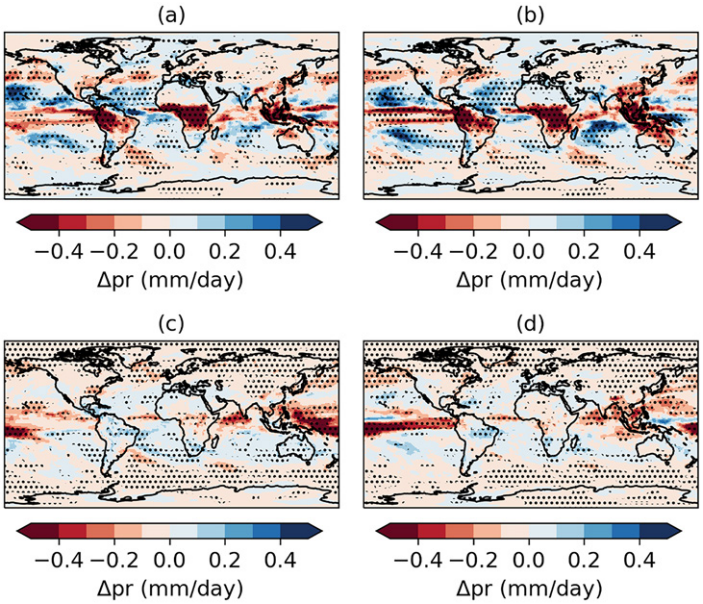

FIG. C6. As in Fig. C5, but for precipitation.

Unauthenticated | Downloaded 02/14/25 09:04 AM UTC

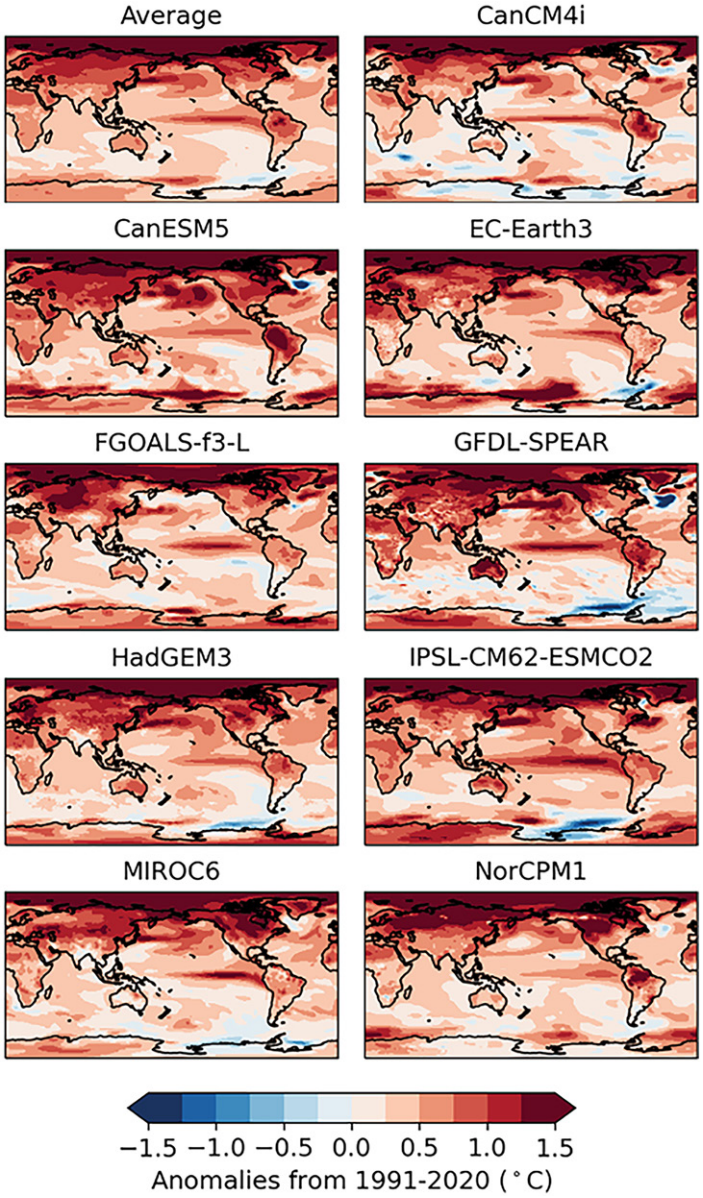

Fig. C7. Predictions of 2023 annual mean anomalies from the 1991 to 2020 average for near-surface air temperature under P1 noVolc for the individual models.

Unauthenticated | Downloaded 02/14/25 09:04 AM UTC

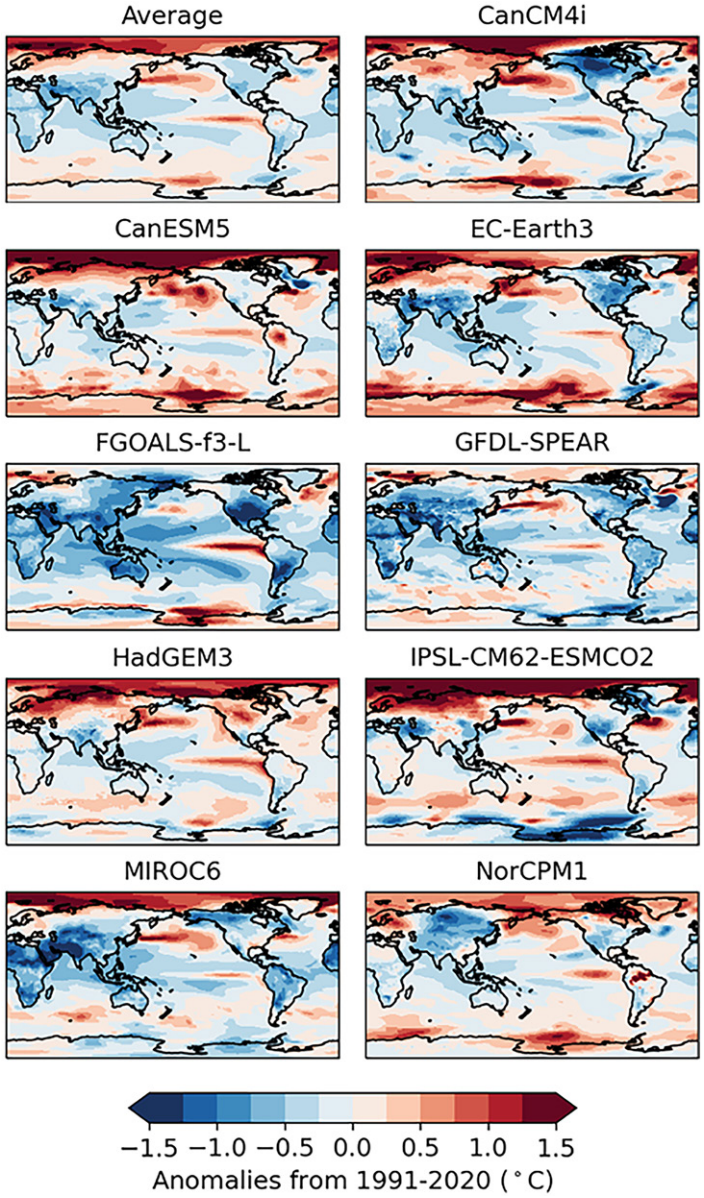

FIG. C8. As in Fig. C7, but for Volc predictions.

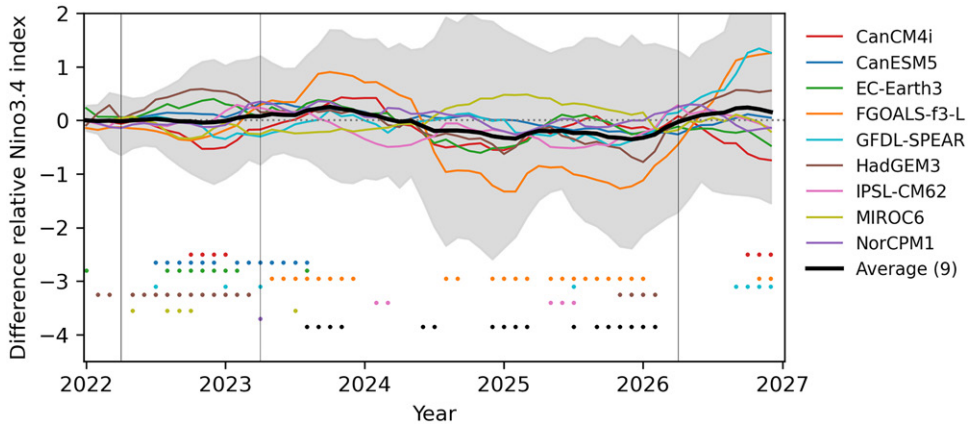

FIG. C9. Monthly relative Niño-3.4 index response (Volc–noVolc) for individual models (color) and the equally weighted multimodel average (black). Values are the difference between those in Figs. 5d and 5c. Shading indicates the 5th–95th percentile ranges of the pooled ensemble. Vertical lines indicate the timings of the posteruption cooling and recovery phases. Color and black dots indicate statistically significant responses at the 95% confidence level for individual models and the multimodel average, respectively (see appendix B).

Unauthenticated | Downloaded 02/14/25 09:04 AM UTC

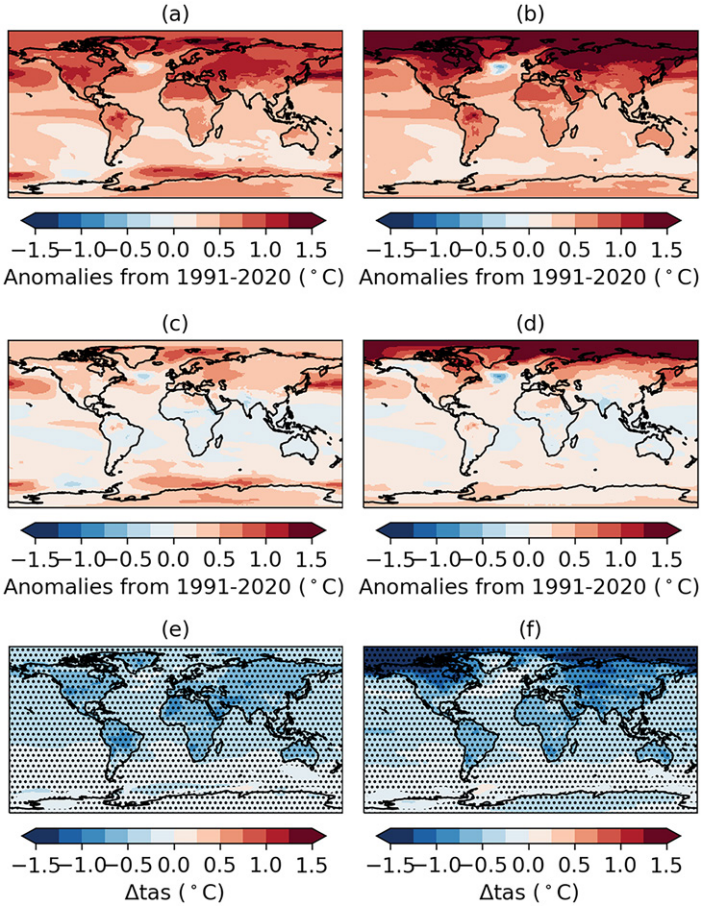

FIG. C10. Multimodel mean predictions for 2022–26 (a),(c) May–September and (b),(d) November–March anomalies from the 1991 to 2020 average for near-surface air temperature under P1 (a),(b) noVolc and (c),(d) Volc. The noVolc forecasts are analogous to the LC-ADCP 2022-issued forecasts, except that the model ensemble is different. (e),(d) Temperature response (Volc–noVolc) for 2022–06 (a),(c) May–September and (b),(d) November–March predictions. Stippling indicates a statistically significant response at the 95% confidence level (see appendix B).

Unauthenticated | Downloaded 02/14/25 09:04 AM UTC

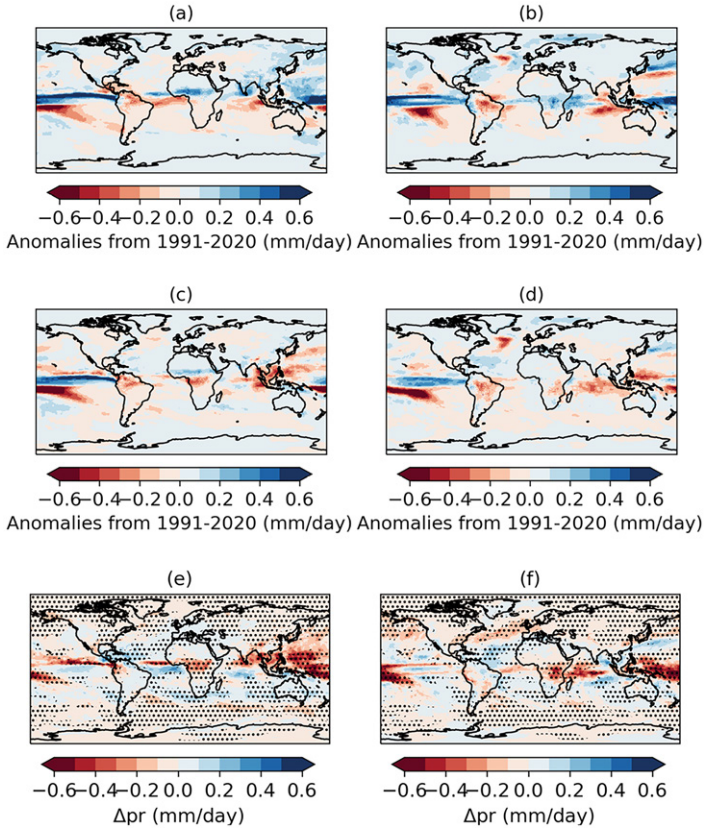

Fig. C11. As in Fig. C10, but for precipitation.

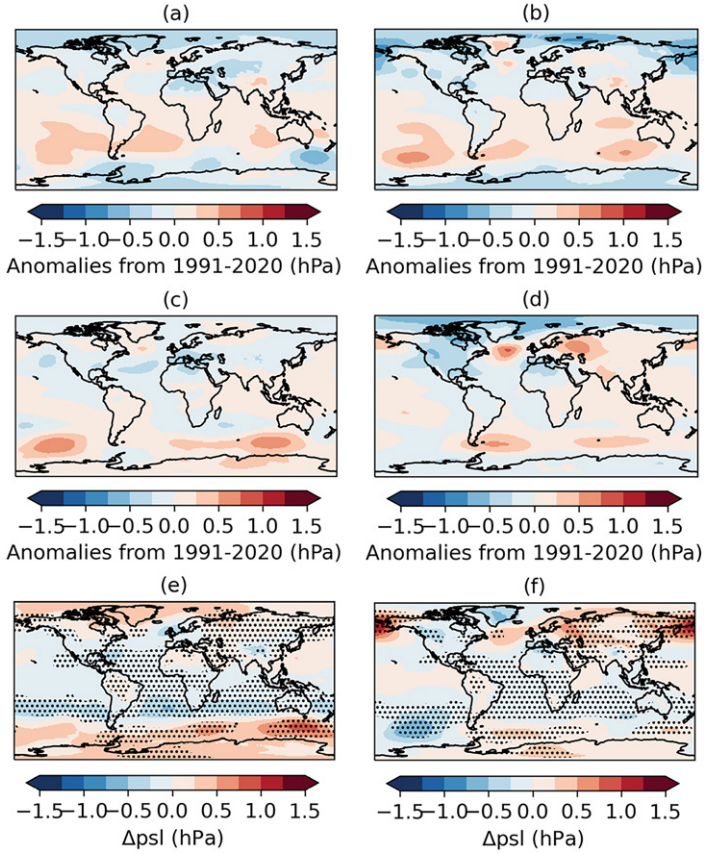

Fig. C12. As in Fig. C10, but for sea level pressure.

Unauthenticated | Downloaded 02/14/25 09:04 AM UTC

References

Adams, B. J., M. E. Mann, and C. M. Ammann, 2003: Proxy evidence for an El Niño-like response to volcanic forcing. *Nature*, **426**, 274–278, https://doi.org/10.1038/nature02101.

Aubry, T. J., M. Toohey, L. Marshall, A. Schmidt, and A. M. Jellinek, 2020: A new volcanic stratospheric sulfate aerosol forcing emulator (EVA_H): Comparison with interactive stratospheric aerosol models. *J. Geophys. Res. Atmos.*, **125**, e2019JD031303, https://doi.org/10.1029/2019JD031303.

Azoulay, A., H. Schmidt, and C. Timmreck, 2021: The Arctic polar vortex response to volcanic forcing of different strengths. *J. Geophys. Res. Atmos.*, **126**, e2020JD034450, https://doi.org/10.1029/2020JD034450.

Bethke, I., S. Outten, O. H. Otterå, E. Hawkins, S. Wagner, M. Sigl, and P. Thorne, 2017: Potential volcanic impacts on future climate variability. *Nat. Climate Change*, **7**, 799–805, https://doi.org/10.1038/nclimate3394.

——, and Coauthors, 2021: NorCPM1 and its contribution to CMIP6 DCPP. *Geosci. Model Dev.*, **14**, 7073–7116, https://doi.org/10.5194/gmd-14-7073-2021.

Bilbao, R., and Coauthors, 2021: Assessment of a full-field initialized decadal climate prediction system with the CMIP6 version of EC-Earth. *Earth Syst. Dyn.*, **12**, 173–196, https://doi.org/10.5194/esd-12-173-2021.

——, and Coauthors, 2024: Impact of volcanic eruptions on CMIP6 decadal predictions: A multi-model analysis. *Earth Syst. Dyn.*, **15**, 501–525, https://doi.org/10.5194/esd-15-501-2024.

Bittner, M., H. Schmidt, C. Timmreck, and F. Sienz, 2016: Using a large ensemble of simulations to assess the Northern Hemisphere stratospheric dynamical response to tropical volcanic eruptions and its uncertainty. *Geophys. Res. Lett.*, **43**, 9324–9332, https://doi.org/10.1002/2016GL070587.

Boer, G. J., V. V. Kharin, and W. J. Merryfield, 2013: Decadal predictability and forecast skill. *Climate Dyn.*, **41**, 1817–1833, https://doi.org/10.1007/s00382-013-1705-0.

——, and Coauthors, 2016: The Decadal Climate Prediction Project (DCPP) contribution to CMIP6. *Geosci. Model Dev.*, **9**, 3751–3777, https://doi.org/10.5194/gmd-9-3751-2016.

Carn, S., 2022: Multi-satellite volcanic sulfur dioxide L4 long-term global database V4. Goddard Earth Science Data and Information Services Center (GES DISC), accessed 22 December 2023, https://doi.org/10.5067/MEASURES/SO2/DATA405.

Christiansen, B., 2008: Volcanic eruptions, large-scale modes in the Northern Hemisphere, and the El Niño–Southern Oscillation. *J. Climate*, **21**, 910–922, https://doi.org/10.1175/2007JCLI1657.1.

Clyne, M., and Coauthors, 2021: Model physics and chemistry causing intermodel disagreement within the VolMIP-Tambora interactive stratospheric aerosol ensemble. *Atmos. Chem. Phys.*, **21**, 3317–3343, https://doi.org/10.5194/acp-21-3317-2021.

Cruz-García, R., P. Ortega, V. Guemas, J. C. Acosta-Navarro, F. Massonnet, and F. J. Doblas-Reyes, 2021: An anatomy of Arctic sea ice forecast biases in the seasonal prediction system with EC-Earth. *Climate Dyn.*, **56**, 1799–1813, https://doi.org/10.1007/s00382-020-05560-4.

DallaSanta, K., and L. M. Polvani, 2022: Volcanic stratospheric injections up to 160 Tg(S) yield a Eurasian winter warming indistinguishable from internal variability. *Atmos. Chem. Phys.*, **22**, 8843–8862, https://doi.org/10.5194/acp-22-8843-2022.

DiNezio, P. N., C. Deser, Y. Okumura, and A. Karspeck, 2017: Predictability of 2-year La Niña events in a coupled general circulation model. *Climate Dyn.*, **49**, 4237–4261, https://doi.org/10.1007/s00382-017-3575-3.

Dogar, M. M., and Coauthors, 2023: A review of El Niño Southern Oscillation linkage to strong volcanic eruptions and post-volcanic winter warming. *Earth Syst. Environ.*, **7**, 15–42, https://doi.org/10.1007/s41748-022-00331-z.

Dunn, R. J. H., and Coauthors, 2022: Global climate. *Bull. Amer. Meteor. Soc.*, **103**, S11–S142, https://doi.org/10.1175/BAMS-D-22-0092.1.

Dunstone, N., and Coauthors, 2022: Towards useful decadal climate services. *Bull. Amer. Meteor. Soc.*, **103**, E1705–E1719, https://doi.org/10.1175/BAMS-D-21-0190.1.

Estella-Perez, V., J. Mignot, E. Guilyardi, D. Swingedouw, and G. Reverdin, 2020: Advances in reconstructing the AMOC using sea surface observations of salinity. *Climate Dyn.*, **55**, 975–992, https://doi.org/10.1007/s00382-020-05304-4.

Freychet, N., A. P. Schurer, A. P. Ballinger, L. Suarez-Gutierrez, and C. Timmreck, 2023: Assessing the impact of very large volcanic eruptions on the risk of extreme climate events. *Environ. Res. Climate*, **2**, 035015, https://doi.org/10.1088/2752-5295/acee9f.

Gonzalez, P. L. M., and L. Goddard, 2016: Long-lead ENSO predictability from CMIP5 decadal hindcasts. *Climate Dyn.*, **46**, 3127–3147, https://doi.org/10.1007/s00382-015-2757-0.

Gu, G., and R. F. Adler, 2011: Precipitation and temperature variations on the interannual time scale: Assessing the impact of ENSO and volcanic eruptions. *J. Climate*, **24**, 2258–2270, https://doi.org/10.1175/2010JCLI3727.1.

Gulev, S. K., and Coauthors, 2021: Changing state of the climate system. *Climate Change 2021: The Physical Science Basis*, V. Masson-Delmotte et al., Eds., Cambridge University Press, 287–422, https://doi.org/10.1017/9781009157896.004.

Guo, S., G. J. S. Bluth, W. I. Rose, I. M. Watson, and A. J. Prata, 2004: Re-evaluation of SO_2 release of the 15 June 1991 Pinatubo eruption using ultraviolet and infrared satellite sensors. *Geochem. Geophys. Geosyst.*, **5**, Q04001, https://doi.org/10.1029/2003GC000654.

Haywood, J. M., A. Jones, N. Bellouin, and D. Stephenson, 2013: Asymmetric forcing from stratospheric aerosols impacts Sahelian rainfall. *Nat. Climate Change*, **3**, 660–665, https://doi.org/10.1038/nclimate1857.

Hermanson, L., and Coauthors, 2020: Robust multiyear climate impacts of volcanic eruptions in decadal prediction systems. *J. Geophys. Res. Atmos.*, **125**, e2019JD031739, https://doi.org/10.1029/2019JD031739.

——, and Coauthors, 2022: WMO global annual to decadal climate update: A prediction for 2021–2025. *Bull. Amer. Meteor. Soc.*, **103**, E1117–E1129, https://doi.org/10.1175/BAMS-D-20-0311.1.

Hersbach, H., and Coauthors, 2020: The ERA5 global reanalysis. *Quart. J. Roy. Meteor. Soc.*, **146**, 1999–2049, https://doi.org/10.1002/qj.3803.

Hu, S., and Coauthors, 2023: CAS FGOALS-f3-L model datasets for CMIP6 DCPP experiment. *Adv. Atmos. Sci.*, **40**, 1911–1922, https://doi.org/10.1007/s00376-023-2122-x.

Iles, C. E., and G. C. Hegerl, 2014: The global precipitation response to volcanic eruptions in the CMIP5 models. *Environ. Res. Lett.*, **9**, 104012, https://doi.org/10.1088/1748-9326/9/10/104012.

——, ——, A. P. Schurer, and X. Zhang, 2013: The effect of volcanic eruptions on global precipitation. *J. Geophys. Res. Atmos.*, **118**, 8770–8786, https://doi.org/10.1002/jgrd.50678.

Illing, S., C. Kadow, H. Pohlmann, and C. Timmreck, 2018: Assessing the impact of a future volcanic eruption on decadal predictions. *Earth Syst. Dyn.*, **9**, 701–715, https://doi.org/10.5194/esd-9-701-2018.

Jenkins, S., C. Smith, M. Allen, and R. Grainger, 2023: Tonga eruption increases chance of temporary surface temperature anomaly above 1.5°C. *Nat. Climate Change*, **13**, 127–129, https://doi.org/10.1038/s41558-022-01568-2.

Jones, C. D., and Coauthors, 2021: The climate response to emissions reductions due to COVID-19: Initial results from CovidMIP. *Geophys. Res. Lett.*, **48**, e2020GL091883, https://doi.org/10.1029/2020GL091883.

Kataoka, T., and Coauthors, 2020: Seasonal to decadal predictions with MIROC6: Description and basic evaluation. *J. Adv. Model. Earth Syst.*, **12**, e2019MS002035, https://doi.org/10.1029/2019MS002035.

Khodri, M., and Coauthors, 2017: Tropical explosive volcanic eruptions can trigger El Niño by cooling tropical Africa. *Nat. Commun.*, **8**, 778, https://doi.org/10.1038/s41467-017-00755-6.

Liu, Y., M. G. Donat, M. H. England, L. V. Alexander, A. L. Hirsch, and C. Delgado-Torres, 2023: Enhanced multi-year predictability after El Niño and La Niña events. *Nat. Commun.*, **14**, 6387, https://doi.org/10.1038/s41467-023-42113-9.

Lücke, L. J., A. P. Schurer, M. Toohey, L. R. Marshall, and G. C. Hegerl, 2023: The effect of uncertainties in natural forcing records on simulated temperature

Unauthenticated | Downloaded 02/14/25 09:04 AM UTC

during the last millennium. *Climate Past*, **19**, 959–978, https://doi.org/10.5194/cp-19-959-2023.

Luo, B., 2018a: Stratospheric aerosol data for use in CMIP6 models. ftp://iacftp.ethz.ch/pub_read/luo/CMIP6/Readme_Data_Description.pdf.

——, 2018b: Release Notes Stratospheric Aerosol Radiative Forcing and SAD version v4.0.01850—2016. ftp://iacftp.ethz.ch/pub_read/luo/CMIP6_SAD_radForcing_v4.0.0/Release_note_v4.0.0.pdf.

Maher, N., S. McGregor, M. H. England, and A. Sen Gupta, 2015: Effects of volcanism on tropical variability. *Geophys. Res. Lett.*, **42**, 6024–6033, https://doi.org/10.1002/2015GL064751.

McGregor, S., and A. Timmermann, 2011: The effect of explosive tropical volcanism on ENSO. *J. Climate*, **24**, 2178–2191, https://doi.org/10.1175/2010JCLI3990.1.

——, M. Khodri, N. Maher, M. Ohba, F. S. R. Pausata, and S. Stevenson, 2020: The effect of strong volcanic eruptions on ENSO. *El Niño Southern Oscillation in a Changing Climate*, *Geophys. Monogr.*, Vol. 253, M. J. McPhaden, A. Santoso, and W. Cai, Eds., Amer. Geophys. Union, 267–287, https://doi.org/10.1002/9781119548164.ch12.

Merryfield, W. J., and Coauthors, 2013: The Canadian Seasonal to Interannual Prediction System. Part I: Models and initialization. *Mon. Wea. Rev.*, **141**, 2910–2945, https://doi.org/10.1175/MWR-D-12-00216.1.

Miao, J. P., T. Wang, H. J. Wang, and J. Q. Sun, 2018: Interannual weakening of the tropical Pacific Walker circulation due to strong tropical volcanism. *Adv. Atmos. Sci.*, **35**, 645–658, https://doi.org/10.1007/s00376-017-7134-y.

Mignot, J., M. Khodri, C. Frankignoul, and J. Servonnat, 2011: Volcanic impact on the Atlantic Ocean over the last millennium. *Climate Past*, **7**, 1439–1455, https://doi.org/10.5194/cp-7-1439-2011.

Millán, L., and Coauthors, 2022: The Hunga Tonga-Hunga Ha'apai hydration of the stratosphere. *Geophys. Res. Lett.*, **49**, e2022GL099381, https://doi.org/10.1029/2022GL099381.

Ohba, M., H. Shiogama, T. Yokohata, and M. Watanabe, 2013: Impact of strong tropical volcanic eruptions on ENSO simulated in a coupled GCM. *J. Climate*, **26**, 5169–5182, https://doi.org/10.1175/JCLI-D-12-00471.1.

O'Kane, T. J., and Coauthors, 2023: Recent applications and potential of near-term (interannual to decadal) climate predictions. *Front. Climate*, **5**, 1121626, https://doi.org/10.3389/fclim.2023.1121626.

Oman, L., A. Robock, G. Stenchikov, G. A. Schmidt, and R. Ruedy, 2005: Climatic response to high-latitude volcanic eruptions. *J. Geophys. Res.*, **110**, D13103, https://doi.org/10.1029/2004JD005487.

Paik, S., and S.-K. Min, 2018: Assessing the impact of volcanic eruptions on climate extremes using CMIP5 models. *J. Climate*, **31**, 5333–5349, https://doi.org/10.1175/JCLI-D-17-0651.1.

——, ——, and S.-I. An, 2022: How explosive volcanic eruptions reshape daily precipitation distributions. *Wea. Climate Extremes*, **37**, 100489, https://doi.org/10.1016/j.wace.2022.100489.

——, ——, S.-W. Son, E.-P. Lim, S. McGregor, S.-I. An, J.-S. Kug, and S.-W. Yeh, 2023: Impact of volcanic eruptions on extratropical atmospheric circulations: Review, revisit and future directions. *Environ. Res. Lett.*, **18**, 063003, https://doi.org/10.1088/1748-9326/acd5e6.

Pausata, F. S. R., L. Chafik, R. Caballero, and D. S. Battisti, 2015: Impacts of high-latitude volcanic eruptions on ENSO and AMOC. *Proc. Natl. Acad. Sci. USA*, **112**, 13 784–13 788, https://doi.org/10.1073/pnas.1509153112.

——, C. Karamperidou, R. Caballero, and D. S. Battisti, 2016: ENSO response to high-latitude volcanic eruptions in the Northern Hemisphere: The role of the initial conditions. *Geophys. Res. Lett.*, **43**, 8694–8702, https://doi.org/10.1002/2016GL069575.

——, D. Zanchettin, K. Christina, R. Caballero, and D. S. Battisti, 2020: ITCZ shift and extratropical teleconnections drive ENSO response to volcanic eruptions. *Sci. Adv.*, **6**, eaaz5006, https://doi.org/10.1126/sciadv.aaz5006.

Predybaylo, E., G. L. Stenchikov, A. T. Wittenberg, and F. Zeng, 2017: Impacts of a Pinatubo-size volcanic eruption on ENSO. *J. Geophys. Res. Atmos.*, **122**, 925–947, https://doi.org/10.1002/2016JD025796.

——, G. Stenchikov, A. T. Wittenberg, and S. Osipov, 2020: El Niño/Southern Oscillation response to low-latitude volcanic eruptions depends on ocean pre-conditions and eruption timing. *Commun. Earth Environ.*, **1**, 12, https://doi.org/10.1038/s43247-020-0013-y.

Quaglia, I., and Coauthors, 2023: Interactive stratospheric aerosol models' response to different amounts and altitudes of SO_2 injection during the 1991 Pinatubo eruption. *Atmos. Chem. Phys.*, **23**, 921–948, https://doi.org/10.5194/acp-23-921-2023.

Robock, A., and J. Mao, 1992: Winter warming from large volcanic eruptions. *Geophys. Res. Lett.*, **19**, 2405–2408, https://doi.org/10.1029/92GL02627.

——, and ——, 1995: The volcanic signal in surface temperature observations. *J. Climate*, **8**, 1086–1103, https://doi.org/10.1175/1520-0442(1995)008<1086:TVSIST>2.0.CO;2.

Samelson, R. M., and E. Tziperman, 2001: Instability of the chaotic ENSO: The growth-phase predictability barrier. *J. Atmos. Sci.*, **58**, 3613–3625, https://doi.org/10.1175/1520-0469(2001)058<3613:IOTCET>2.0.CO;2.

Sato, M., E. J. Hansen, M. P. McCormick, and J. B. Pollack, 1993: Stratospheric aerosol optical depths, 1850–1990. *J. Geophys. Res.*, **98**, 22 987–22 994, https://doi.org/10.1029/93JD02553.

Schoeberl, M. R., Y. Wang, R. Ueyama, A. Dessler, G. Taha, and W. Yu, 2023: The estimated climate impact of the Hunga Tonga-Hunga Ha'apai eruption plume. *Geophys. Res. Lett.*, **50**, e2023GL104634, https://doi.org/10.1029/2023GL104634.

Schurer, A. P., S. F. B. Tett, and G. C. Hegerl, 2014: Small influence of solar variability on climate over the past millennium. *Nat. Geosci.*, **7**, 104–108, https://doi.org/10.1038/ngeo2040.

Sellar A. A., and Coauthors, 2020: Implementation of U.K. Earth system models for CMIP6. *J. Adv. Model. Earth Syst.*, **12**, e2019MS001946, https://doi.org/10.1029/2019MS001946.

Sharmila, S., H. Hendon, O. Alves, A. Weisheimer, and M. Balmaseda, 2023: Contrasting El Niño–La Niña predictability and prediction skill in 2-year reforecasts of the twentieth century. *J. Climate*, **36**, 1269–1285, https://doi.org/10.1175/JCLI-D-22-0028.1.

Shindell, D. T., G. A. Schmidt, M. E. Mann, and G. Faluvegi, 2004: Dynamic winter climate response to large tropical volcanic eruptions since 1600. *J. Geophys. Res.*, **109**, D05104, https://doi.org/10.1029/2003JD004151.

Sospedra-Alfonso, R., W. J. Merryfield, G. J. Boer, V. V. Kharin, W.-S. Lee, C. Seiler, and J. R. Christian, 2021: Decadal climate predictions with the Canadian Earth System Model version 5 (CanESM5). *Geosci. Model Dev.*, **14**, 6863–6891, https://doi.org/10.5194/gmd-14-6863-2021.

Stenchikov, G., A. Robock, V. Ramaswamy, M. D. Schwarzkopf, K. Hamilton, and S. Ramachandran, 2002: Arctic Oscillation response to the 1991 Mount Pinatubo eruption: Effects of volcanic aerosols and ozone depletion. *J. Geophys. Res.*, **107**, 4803, https://doi.org/10.1029/2002JD002090.

——, K. Hamilton, R. J. Stouffer, A. Robock, V. Ramaswamy, B. Santer, and H.-F. Graf, 2006: Arctic Oscillation response to volcanic eruptions in the IPCC AR4 climate models. *J. Geophys. Res.*, **111**, D07107, https://doi.org/10.1029/2005JD006286.

Sun, W., B. Wang, J. Liu, D. Chen, C. Gao, L. Ning, and L. Chen, 2019: How northern high-latitude volcanic eruptions in different seasons affect ENSO. *J. Climate*, **32**, 3245–3262, https://doi.org/10.1175/JCLI-D-18-0290.1.

Swingedouw, D., J. Mignot, P. Ortega, M. Khodri, M. Menegoz, C. Cassou, and V. Hanquiez, 2017: Impact of explosive volcanic eruptions on the main climate variability modes. *Global Planet. Change*, **150**, 24–45, https://doi.org/10.1016/j.gloplacha.2017.01.006.

Thomason, L. W., and Coauthors, 2018: A global space-based stratospheric aerosol climatology: 1979–2016. *Earth Syst. Sci. Data*, **10**, 469–492, https://doi.org/10.5194/essd-10-469-2018.

Timmreck, C., D. Olonscheck, A. P. Ballinger, R. d'Agostino, S.-W. Fang, A. P. Schurer, and G. C. Hegerl, 2024: Linearity of the climate response to increasingly strong tropical volcanic eruptions in a large ensemble framework. *J. Climate*, **37**, 2455–2470, https://doi.org/10.1175/JCLI-D-23-0408.1.

Unauthenticated | Downloaded 02/14/25 09:04 AM UTC

Toohey, M., and M. Sigl, 2017: Volcanic stratospheric sulfur injections and aerosol optical depth from 500 BCE to 1900 CE. *Earth Syst. Sci. Data*, **9**, 809–831, https://doi.org/10.5194/essd-9-809-2017.

——, B. Stevens, H. Schmidt, and C. Timmreck, 2016: Easy Volcanic Aerosol (EVA v1.0): An idealized forcing generator for climate simulations. *Geosci. Model Dev.*, **9**, 4049–4070, https://doi.org/10.5194/gmd-9-4049-2016.

van Oldenborgh, G. J., H. Hendon, T. Stockdale, M. L'Heureux, E. C. de Perez, R. Singh, and M. van Aalst, 2021: Defining El Niño indices in a warming climate. *Environ. Res. Lett.*, **16**, 044003, https://doi.org/10.1088/1748-9326/abe9ed.

Vernier, J.-P., and Coauthors, 2024: The 2019 Raikoke eruption as a testbed used by the Volcano Response group for rapid assessment of volcanic atmospheric impacts. *Atmos. Chem. Phys.*, **24**, 5765–5782, https://doi.org/10.5194/acp-24-5765-2024.

Wang, T., J. Miao, H. Wang, and J. Sun, 2021: Influence of strong tropical volcanic eruptions on daily temperature and precipitation extremes across the globe. *J. Meteor. Res.*, **35**, 428–443, https://doi.org/10.1007/s13351-021-0160-9.

Ward, B., F. S. R. Pausata, and N. Maher, 2021: The sensitivity of the El Niño–Southern Oscillation to volcanic aerosol spatial distribution in the MPI Grand Ensemble. *Earth Syst. Dyn.*, **12**, 975–996, https://doi.org/10.5194/esd-12-975-2021.

WMO, 2022: WMO Global Annual to Decadal Climate Update. Target years: 2022 and 2022–2026. WMO Update, 24 pp., https://library.wmo.int/idurl/4/56318.

——, 2023: WMO Global Annual to Decadal Climate Update. Target years: 2023 and 2023–2027. WMO Update, 24 pp., https://library.wmo.int/idurl/4/66224.

Wu, B., T. Zhou, and F. Zheng, 2018: EnOI-IAU initialization scheme designed for decadal climate prediction system IAP-DecPreS. *J. Adv. Model. Earth Syst.*, **10**, 342–356, https://doi.org/10.1002/2017MS001132.

Yang, X., and Coauthors, 2021: On the development of GFDL's decadal prediction system: Initialization approaches and retrospective forecast assessment. *J. Adv. Model. Earth Syst.*, **13**, e2021MS002529, https://doi.org/10.1029/2021MS002529.

Yeager, S. G., and Coauthors, 2022: The Seasonal-to-Multiyear Large Ensemble (SMYLE) prediction system using the Community Earth System Model version 2. *Geosci. Model Dev.*, **15**, 6451–6493, https://doi.org/10.5194/gmd-15-6451-2022.

Zambri, B., and A. Robock, 2016: Winter warming and summer monsoon reduction after volcanic eruptions in Coupled Model Intercomparison Project 5 (CMIP5) simulations. *Geophys. Res. Lett.*, **43**, 10 920–10 928, https://doi.org/10.1002/2016GL070460.

——, A. N. LeGrande, A. Robock, and J. Slawinska, 2017: Northern Hemisphere winter warming and summer monsoon reduction after volcanic eruptions over the last millennium. *J. Geophys. Res. Atmos.*, **112**, 7971–7989, https://doi.org/10.1002/2017JD026728.

Zanchettin, D., C. Timmreck, H.-F. Graf, A. Rubino, S. Lorenz, K. Lohmann, K. Kruger, and J. H. Jungclaus, 2012: Bi-decadal variability excited in the coupled ocean–atmosphere system by strong tropical volcanic eruptions. *Climate Dyn.*, **39**, 419–444, https://doi.org/10.1007/s00382-011-1167-1.

——, and Coauthors, 2016: The Model Intercomparison Project on the climatic response to Volcanic forcing (VolMIP): Experimental design and forcing input data for CMIP6. *Geosci. Model Dev.*, **9**, 2701–2719, https://doi.org/10.5194/gmd-9-2701-2016.

——, C. Timmreck, M. Toohey, J. H. Jungclaus, M. Bittner, S. J. Lorenz, and A. Rubino, 2019: Clarifying the relative role of forcing uncertainties and initial-condition unknowns in spreading the climate response to volcanic eruptions. *Geophys. Res. Lett.*, **46**, 1602–1611, https://doi.org/10.1029/2018GL081018.

——, and Coauthors, 2022: Effects of forcing differences and initial conditions on inter-model agreement in the VolMIP volc-pinatubo-full experiment. *Geosci. Model Dev.*, **15**, 2265–2292, https://doi.org/10.5194/gmd-15-2265-2022.

Zhu, Y., and Coauthors, 2022: Perturbations in stratospheric aerosol evolution due to the water-rich plume of the 2022 Hunga-Tonga eruption. *Comm. Earth Environ.*, **3**, 248, https://doi.org/10.1038/s43247-022-00580-w.

Zuo, M., W. Man, T. Zhou, and Z. Guo, 2018: Different impacts of northern, tropical, and southern volcanic eruptions on the tropical Pacific SST in the last millennium. *J. Climate*, **31**, 6729–6744, https://doi.org/10.1175/JCLI-D-17-0571.1.

——, T. Zhou, and W. Man, 2019: Wetter global arid regions driven by volcanic eruptions. *J. Geophys. Res. Atmos.*, **124**, 13 648–13 662, https://doi.org/10.1029/2019JD031171.

——, W. Man, and T. Zhou, 2021: Dependence of global monsoon response to volcanic eruptions on the background oceanic states. *J. Climate*, **34**, 8273–8289, https://doi.org/10.1175/JCLI-D-20-0891.1.

Unauthenticated | Downloaded 02/14/25 09:04 AM UTC